Loss of EED in the oocyte causes initial fetal growth restriction followed by placental hyperplasia and offspring overgrowth.

Short title: *Epigenetic regulation of fetal growth restriction, placental expansion and offspring overgrowth*

Authors: Ruby Oberin[1#], Sigrid Petautschnig[1#], Tesha Tsai[1^], Zhipeng Qu[2], Ellen G. Jarred[1], Heidi Bildsoe[1], Thi T. Truong[3], Dilini Fernando[1], Maarten van den Buuse[4], David K. Gardner[3], Natalie A. Sims[5], David L. Adelson[2] and Patrick S. Western[1]*

Affiliations: [1]Centre for Reproductive Health, Hudson Institute of Medical Research and Department of Molecular and Translational Science, Monash University, Clayton, Victoria, Australia; [2]Department of Bioinformatics and Computational Genetics, School of Biological Sciences, University of Adelaide, Adelaide, South Australia, Australia; [3]School of BioSciences, University of Melbourne, Parkville, Victoria, Australia; [4]School of Psychology and Public Health, La Trobe University, Melbourne, Victoria, Australia; [5]Bone Cell Biology and Disease Unit, St. Vincent's Institute of Medical Research and Department of Medicine at St. Vincent's Hospital, Fitzroy, Victoria, Australia.

* Corresponding author: patrick.western@hudson.org.au

[#] These authors contributed equally to this work

^Current Address: School of Health and Biomedical Sciences, RMIT University, Bundoora, Victoria, Australia.

Abstract

Germline epigenetic programming, including genomic imprinting, substantially influences offspring development. Polycomb Repressive Complex 2 (PRC2) plays an important role in Histone 3 Lysine 27 trimethylation (H3K27me3)-dependent imprinting, loss of which leads to placental hyperplasia in mammalian offspring generated by somatic cell nuclear transfer (SCNT). In this study, we show that offspring from mouse oocytes lacking the Polycomb protein Embryonic Ectoderm Development (EED) were initially growth restricted, characterised by low blastocyst cell counts and substantial mid-gestational developmental delay. However, this initial delay was remediated by striking late-gestational placental hyperplasia, closely followed by rapid fetal catch-up growth and subsequent overgrowth. Remodelling of the placenta involved expansion of fetal and maternal tissues, including conspicuous expansion of the glycogen enriched cell population in the junctional zone.

Genome-wide analyses identified extensive transcriptional dysregulation in affected placentas, including a range of imprinted and non-imprinted genes. Our data demonstrate that altered PRC2-dependent programming in the oocyte elicits complex program of fetal growth restriction followed by placental hyperplasia, which drives catchup growth that ultimately results in perinatal offspring overgrowth.

Introduction

Epigenetic mechanisms orchestrate tissue development, body patterning and growth by regulating chromatin accessibility and expression of developmental genes in embryonic and extraembryonic tissues (1, 2). Histone 3 Lysine 27 trimethylation (H3K27me3) is a repressive epigenetic modification catalysed by Polycomb Repressive Complex 2 (PRC2), which is composed of core components, EED, EZH1/2 and SUZ12, all of which are essential for histone methyltransferase activity (3-6). Global deletion of any of the individual genes encoding these PRC2 subunits results in embryonic lethality in mice, while conditional deletions of *Eed, Ezh2* or *Suz12* result in altered patterning and organ function in a range of tissues (3-5, 7-13). In humans, *de novo* germline mutations in *EED, EZH2* or *SUZ12* result in Cohen Gibson, Weaver and Imagawa-Matsumoto syndromes, which all involve overgrowth, skeletal dysmorphologies and cognitive abnormalities in patients (14-20).

In mouse oocytes, PRC2 is required for non-canonical H3K27me3-imprinting, whereby H3K27me3 silences the maternal allele of several genes resulting in paternal allele-specific expression of the affected genes in pre-implantation embryos and extraembryonic tissues (21, 22). Oocyte-specific deletion of *Eed* using *Gdf9Cre* resulted in loss of H3K27me3-imprinting in preimplantation embryos and extraembryonic ectoderm with growth restriction and male-biased lethality in mid-gestation offspring (23). However, in contrast to growth restriction, another study that employed a similar strategy using *Zp3Cre* to delete *Eed* in oocytes found that postnatal offspring were overgrown (7). Moreover, somatic cell nuclear transfer (SCNT) embryos lack H3K27me3-imprinting, resulting in in bi-allelic expression of several genes that has been linked to placental hyperplasia and fetal overgrowth(24-27).

71 We proposed that loss of EED in the oocyte sets up a developmental trajectory that involves
72 initial fetal growth restriction that is resolved by placentally driven catch-up growth, which
73 would explain the apparent stage-dependent discrepancy in the literature. We demonstrate
74 that while fetuses derived from *Eed* null oocytes were initially growth restricted, they
75 underwent rapid late-gestational catch-up growth that culminated in postnatal overgrowth.
76 Detailed analysis of the placenta suggests this complex growth curve is supported by placental
77 expansion and increased placental efficiency late in gestation. Ultimately, this work reveals a
78 critical role for EED in the oocyte for regulating a complex program of fetal and placental
79 growth and function in offspring, and that when EED function is lost in oocytes, placental
80 hyperplasia drives offspring catchup growth so that growth restriction is ameliorated by
81 birth.
82
83 **Results**
84 **Loss of maternal EED compromised mid-gestation survival in offspring**.
85 Previous studies demonstrated apparently contradictory findings in that deletion of *Eed* in
86 oocytes resulted in early embryonic growth restriction (23) and early postnatal offspring
87 overgrowth (7). To understand how these outcomes are realised, we produced offspring from
88 pure C57BL6 females producing *Eed*-homozygous null (*hom*), *Eed* heterozygous (*het*) or *Eed*
89 wild type (*wt*) oocytes and assessed their growth and development throughout the whole
90 gestational period. Initially, $Eed^{fl/fl}$ or $Eed^{fl/wt}$ females were mated to males that were
91 transgenic for *Zp3Cre* to generate females producing *Eed-wt, Eed-het* or *Eed-hom* oocytes (7).
92 Mating of these females to pure C57BL6 *wt* males allowed us to generate isogenic wild type
93 or heterozygous offspring as previously described (Fig. 1A) (7). Heterozygous offspring
94 generated from *Eed* heterozygous oocytes (*HET-het* offspring) or from *Eed* homozygous null
95 oocytes (*HET-hom* offspring) are isogenic. However, the *HET-hom* offspring were generated
96 from oocytes that completely lacked functional EED and the *HET-het* offspring were
97 generated from oocytes that had one functional copy of EED and maintained essentially
98 normal gene repression (7)(Jarred et al., 2022, submitted). As they are isogenic and
99 heterozygous, comparison of *HET-hom* with *HET-het* offspring allowed the identification of
100 differences that resulted specifically from a loss of EED in oocytes in the absence of
101 confounding genetic differences (Fig. 1A). In addition, we generated wild type offspring from
102 *Eed-het* and *Eed-wt* oocytes to compare *WT-wt* and *WT-het* offspring with *HET-het* and *HET-*

103 *hom* offspring, providing controls for differences generated as a result of *Eed* heterozygosity
104 in offspring (Fig. 1A).
105
106 Initially, we used automated time-lapse imaging of individual embryos derived from *Eed-wt*
107 and *Eed-hom* oocytes to track their development from zygote to hatched blastocyst stages.
108 Embryos from *Eed-hom* oocytes reached the 2-cell stage 1.08h earlier than embryos from
109 *Eed-wt* oocytes (Fig. 1B), but blastocyst expansion and hatching took 2.67h longer in *HET-hom*
110 compared to *WT-wt* embryos (Fig. 1C). All other developmental milestones to blastocyst stage
111 were similar between genotypes (Fig. 1B). Although, viability to blastocyst stage was lower in
112 embryos from females producing *Eed-hom* compared to *Eed-wt* oocytes (72.17% vs 88.67%,
113 Fig. 1D), the proportion of embryos surviving to expanded and hatched blastocyst stages did
114 not differ significantly (Supp Fig. 1A).
115
116 To determine whether the cell content of blastocysts was affected, we performed cell counts
117 in whole blastocysts and differential staining of inner cell mass (ICM) and trophectoderm (TE)
118 cells (28)(Supp Fig. 1B). This revealed that overall cell content of embryos from *Eed-hom*
119 females was lower than in *Eed-wt* controls (Fig. 1E). The number of TE cells was not
120 statistically altered, but the ICM contained fewer cells in *HET-hom* embryos compared to *WT-*
121 *wt* controls (Supp Fig. 1C-D). Together, these data indicated that *HET-hom* embryos contained
122 fewer cells overall than controls and that the ICM was smaller in embryos from oocytes that
123 lacked EED compared to oocytes that maintained EED function (Fig. 1F). As previous reports
124 indicated that maternal deletion of *Eed* did not compromise development to the blastocyst
125 stage, or cause apoptosis in blastocysts (23), it is likely that lower proliferation explains the
126 reduction we observed in blastocyst cell number, which affected the ICM rather than the TE.
127
128 To assess the effect of oocyte-specific *Eed* deletion on fetal survival and throughout
129 pregnancy, we compared the number of live fetuses and litter size in offspring generated from
130 *Eed-hom, Eed-het* and *Eed-wt* oocytes at multiple stages during gestation and after birth.
131 Using *Zp3*Cre to delete *Eed* in oocytes, we found no difference between genotypes in the
132 number of implantations of live embryos in four pregnancies from *Eed*-null oocytes analysed
133 at E9.5 (Fig. 1G), indicating that *HET-hom* preimplantation embryos implanted at similar rates
134 and progressed through gastrulation. However, consistent with previous findings (7, 23), the

135 number of live fetuses at E12.5, E14.5, E17.5, and the number of live born pups were both
136 significantly lower for *Eed-hom* mothers than for *Eed-het* and *Eed-wt* control females (Fig.
137 1G). In addition, 71.43% of live fetuses in E17.5 *Eed-hom* pregnancies were female, indicating
138 male-biased lethality of *HET-hom* offspring (Fig. 1H), consistent with previous studies (23, 29).
139
140 **Loss of EED in oocytes results in offspring post-implantation developmental delay with**
141 **catch-up growth and subsequent postnatal overgrowth**.
142 These observations demonstrated that the major period of fetal loss of *HET-hom* offspring
143 was between E9.5 and E12.5 in our model or by E6.5 in Inoue, Chen (23), which indicates that
144 either placental function or embryo survival was compromised in both models. To determine
145 whether differences occurred in the fetus and/or placenta, we assessed the growth and
146 development of surviving mid-late gestation offspring. Embryonic day (E)9.5 *HET-hom*
147 offspring from multiple litters were small compared to *WT-wt* offspring (Fig. 2A). Similarly,
148 E9.5 *HET-hom* offspring, including extraembryonic tissues, were significantly lighter than *HET-*
149 *het, WT-het* and *WT-wt* controls (Supp Fig. 2A). Subsequently, compared to *HET-het, WT-het*
150 and *WT-wt* controls, *HET-hom* embryos contained fewer tail somites at E12.5 and had
151 reduced inter-digital tissue regression in foot plates at E14.5 (Fig. 2B, Supp Fig. 2B),
152 demonstrating that *HET-hom* offspring were developmentally delayed.
153
154 This *in utero* developmental delay contrasted markedly with our previous observation that
155 postnatal *HET-hom* offspring were overgrown at P2 (7). We therefore examined the temporal
156 developmental trajectory of *HET-hom* offspring by measuring fetal weight at E12.5, E14.5 and
157 E17.5 and pup weight on the day of birth (P0) and at P3. While weight of *HET-hom* offspring
158 was significantly lower than *HET-het, WT-het* and *WT-wt* controls at E12.5, E14.5 and E17.5,
159 by P0 and P3 *HET-hom* offspring were heavier than the isogenic *HET-het* controls (Fig. 2C-G).
160 Therefore, while *HET-hom* offspring were initially developmentally delayed and under-weight
161 compared to their isogenic heterozygous counterparts and wild type controls, they
162 underwent rapid catch-up growth between E17.5 and birth and were overgrown by P3 (Supp
163 Fig. 2C), consistent with our previous observations at P2 (7).
164
165 **Oocyte-specific loss of EED results in placental hyperplasia and enhanced placental**
166 **efficiency late in gestation which overlaps with *HET-hom* offspring catch-up growth.**

167 To understand whether the catch-up growth observed in *HET-hom* offspring might be related
168 to changes in placental development, we collected and weighed E12.5, E14.5 and E17.5
169 placentas from *HET-hom, HET-het, WT-het* and *WT-wt* offspring. At E12.5 placental weights
170 were consistent across all genotypes, however at E14.5 *HET-hom* placentas were slightly, but
171 significantly, heavier than *HET-het* controls (Fig. 3A-B). By E17.5 *HET-hom* placentas were 65%
172 heavier than *HET-het* controls (Fig. 3C), a change reflected in differing *HET-hom* and *HET-het*
173 placental growth rates over time (Fig 3D-E). While *HET-hom* and *HET-het* placental growth
174 rates were similar between E12.5 and E14.5, the growth rate of *HET-hom* placentas was 3.29
175 times greater than that of *HET-het* placentas between E14.5 and E17.5 (Fig 3D-E). Moreover,
176 consistent with placental expansion driving fetal growth, comparison of placental to fetal
177 weights revealed that the growth of *HET-hom* placentas immediately preceded the catch-up
178 growth of late-gestation *HET-hom* fetal offspring (Fig. 3D, F). While fetal growth rate was
179 initially low between E12.5 and E14.5 and was similar between E14.5 and E17.5 in *HET-hom*
180 offspring and *HET-het* controls, *HET-hom* offspring gained weight at 1.5 times the rate of *HET-*
181 *het* controls between E17.5 and birth (Fig 3F).
182
183 To further investigate the relationship between placental function and offspring growth, we
184 calculated the offspring body to placental weight ratio, which is indicative of placental
185 efficiency (30). While placental efficiency was consistent across all genotypes at E12.5 (Fig
186 3G), it was substantially increased at E14.5 and E17.5 in *HET-hom* offspring compared to all
187 other genotypes (Fig. 3H-I). Histological sections at E17.5 confirmed that *HET-hom* placentas
188 were obviously larger than *HET-het, WT-het* and *WT-wt* controls. This analysis also revealed
189 that the junctional zone was expanded in *HET-hom* placentas, with abnormal projections of
190 periodic acid-Schiff (PAS)-positive spongiotrophoblast cells into the labyrinth (Fig. 3J).
191
192 **Loss of EED in the oocyte results in altered developmental patterning of the placenta and**
193 **extended gestational length.**
194 Given that PAS staining of E17.5 *HET-hom* placenta indicated substantial changes in placental
195 development, we performed further analyses of *WT-wt*, *WT-het, HET-het* and *HET-hom*
196 placentas at E14.5 and E17.5 using hematoxylin and eosin (H&E) staining. Consistent with the
197 modest increase in weight of *HET-hom* compared to *HET-het* placentas at E14.5 (Fig 3B),
198 quantification of the entire cross-sectional area in H&E-stained sections of E14.5 placentas

199 demonstrated a 19% increase in *HET-hom* placental area compared to *HET-het* controls (Supp
200 Fig. 3A & E). This difference was emphasised in overall cross-sectional area in E17.5 *HET-hom*
201 placentas compared to all other genotypes, with a 55% increase in cross-sectional area
202 compared to *HET-het* controls (Fig. 4A-B). To understand if this increase in placental size was
203 due to changes in a specific layer of the placenta, we measured junctional zone, labyrinth and
204 maternally-derived decidua layer areas. At E14.5, junctional zone area was significantly larger
205 in *HET-hom* placentas compared to the *WT-wt* and *HET-het* controls, however there was no
206 difference the *HET-hom* decidua or labyrinth areas compared to all other genotypes (Supp
207 Fig. 3B-D). At E17.5, the overall cross-sectional area of all layers of *HET-hom* placentas was
208 greater than that of *HET-het* and *WT-wt* controls (Supp Fig 3E-G). However, as a proportion
209 of the total placental area, only the junctional zone was significantly greater for *HET-hom*
210 placentas compared to other genotypes (Fig. 4C-E). Together, these data indicate that the
211 whole *HET-hom* placenta, including the maternal side, is larger than controls. Moreover, this
212 is associated with a disproportionate expansion of the fetally-derived junctional zone
213 between E14.5 and E17.5.
214
215 Closer examination of H&E stained E17.5 placentas also showed that there were significantly
216 more PAS-stained glycogen enriched cells in the junctional zone of *HET-hom* placentas
217 compared to all other genotypes (Fig. 4F-G). As placental glycogen is converted to glucose to
218 support fetal growth, the increased glycogen cell number in *HET-hom* placentas is consistent
219 with a greater glucose requirement in the late gestational fetal catch-up growth observed in
220 the *HET-hom* offspring. In addition to supporting late-gestational fetal growth, placental
221 glycogen stores could support the production of hormones that promote parturition towards
222 the end of the pregnancy (31-34). Consistent with this and the greater numbers of glycogen
223 enriched cells in *HET-hom* placentas, gestational length was extended by 1 day (7/19 litters)
224 or 2 days (5/19 litters) in *Eed-hom* pregnancies compared to the *Eed-wt* and *Eed-het* controls
225 (Fig. 4H). Moreover, in litters where gestational length was extended by one day from 19.5
226 days to 20.5 days, 36.36% of the *HET-hom* offspring were found dead at birth, and in litters
227 where gestational length was extended by two days, all *HET-hom* offspring were found dead
228 at birth. Together, while increased junctional zone area and glycogen cell content
229 corresponded with fetal catch-up growth, it was also linked to increased gestational length in
230 almost 2/3 of all litters.

231

232 **Widespread gene dysregulation occurs in placentas from *Eed-hom* oocytes.**

233 As the developmental changes observed in the placenta indicated that transcriptional
234 regulation may be substantially altered in *HET-hom* placentas we analysed male and female
235 placental tissue from *HET-hom*, *HET-het* and *WT-wt* offspring using RNA-sequencing (RNA-
236 seq). Surprisingly, principal component analysis of the male samples revealed that *HET-hom*
237 placental transcriptomes were indistinct from placental transcriptomes in *HET-het* and *WT-*
238 *wt* controls (Supp Fig 4A), with only one sequence (CAAA01077340.1) differentially expressed
239 between male *HET-hom* and *HET-het* placentas with an FDR<0.05 (false discovery rate) (Supp
240 Fig 4B,). However, since we observed a male bias in fetal mortality in *HET-hom* offspring, the
241 lack of extensive transcriptional differences between the male placental samples may have
242 been influenced by more moderate effects in surviving males. We therefore focussed our
243 analyses on female placentas only. Principal component analysis revealed that the
244 transcriptome of female *HET-hom* placentas were distinct from their counterpart tissues in
245 *HET-het* and *WT-wt* controls (Fig. 5A). Using an FDR<0.05, 2083 differentially expressed genes
246 (DEGs; together referred to as *Eed* placental DEGs) were identified between *HET-hom* vs *HET-*
247 *het* placentas (Fig. 5B, Supp Table 1), and only 4 genes (*Eed*, *Fibin*, *Hapln4* & *Dtx1*) were
248 significantly different between *HET-het* and *WT-wt* placentas. This demonstrated that the vast
249 majority of transcriptional dysregulation in the placenta was not due to heterozygosity of *Eed*
250 but can be best explained by non-genetic effects caused by loss of EED specifically in the
251 oocyte. Gene ontology analysis indicated that the *Eed* placental DEGs are involved in
252 morphogenesis, system development and multicellular organism development (Fig. 5C),
253 suggesting that the gene dysregulation observed in the *HET-hom* placenta influences a diverse
254 range of systems and processes.

255

256 As sequencing was performed on the entire placenta, we compared the *Eed* placental DEG
257 list with published single cell RNA-seq data from E14.5 C57BL/6 placentas as an indication of
258 the placental cell types in which gene dysregulation occurred in our model (35). Although the
259 E14.5 placental stage assessed by Han, Wang (35) was earlier than the E17.5 placental data
260 collected in our analysis, the majority of mature placental cell types are established by E14.5
261 (36). We therefore considered the Han, Wang (35) data useful for predicting the spatial
262 expression for our *Eed* placental DEGs. Of the 2083 *Eed* placental DEGs identified in the *Eed*

263 *HET-hom* placentas, 543 genes were found in the E14.5 mouse placental data set (35). Cell-
264 specific comparisons revealed that of these 543 genes, 166 *Eed* placental DEGs included genes
265 preferentially expressed in the junctional zone and 57 *Eed* placental DEGs were preferentially
266 transcribed in the labyrinth, which we defined as '*Eed* junctional zone DEGs' and '*Eed*
267 labyrinth DEGs', respectively (Fig. 5D-E). In addition, 104 *Eed* placental DEGs included genes
268 preferentially transcribed in the maternally-derived decidua, which we refer to as '*Eed*
269 decidua DEGs' (Fig. 5F). Together these data revealed that gene dysregulation in *HET-hom*
270 placentas was not isolated to a single region, and that both maternal and fetal-derived cells
271 were altered. Of the *Eed* junctional zone DEGs the majority (86.1%) were upregulated,
272 whereas a large proportion of *Eed* labyrinth DEGs and *Eed* decidua DEGs were downregulated
273 (86% and 97.1%, respectively; Fig. 5G-I). Together these data demonstrate a strong bias for
274 up-regulation of genes expressed in the junctional zone layer of the *Eed* placenta. This reflects
275 the significant expansion of the junctional zone as a proportion of the total placental size.
276
277 ***Eed* placental DEGs included both H3K27me3, classically imprinted genes and some X-linked**
278 **genes.**
279 Given the loss of H3K27me3-dependent imprinting at specific genes leads to placental
280 hyperplasia in Somatic Cell Nuclear Transfer (SCNT) embryos we investigated whether
281 imprinted genes were dysregulated in the *Eed HET-hom* placenta. This revealed that of 325
282 known or proposed classically imprinted genes (37, 38), 46 were *Eed* placental DEGs (Fig. 6A,
283 Supp Table 2). Of 76 putative non-canonical H3K27me3 imprinted genes identified by Inoue,
284 Jiang (22), 16 were dysregulated in *HET-hom* placenta (Fig. 6A, Supp Table 1). These included,
285 *Slc38a4*, *Sfmbt2*, *Gab1* and *Smoc1*, for which loss of H3K27me3-dependent imprinting results
286 in placental hyperplasia and/or defective offspring development in SCNT-derived offspring
287 (25-27). Moreover, *Slc38a4, Sfmbt2, Gab1 and Smoc1* were all up-regulated in *HET-hom*
288 placenta, suggesting a loss of H3K27me3-imprinting and abnormal expression of the maternal
289 allele of these genes (Fig. 6B). As a range of classically imprinted genes are also aberrantly
290 expressed in placental cells of SCNT-derived pregnancies (27), we also determined the overlap
291 of *Eed* placental DEGs with imprinted genes that were dysregulated in SCNT placentas. Of the
292 325 classically imprinted genes(37, 38), nine were commonly dysregulated (5 up-regulated
293 and 4 down-regulated) in *HET-hom* placentas and SCNT derived placental cells. In addition,

294 the H3K27me3-imprinted genes *Sfmbt2*, *Slc38a4, Smoc1* and *Gab1* were all upregulated in
295 *Eed HET-hom* placentas, but only *Sfmbt2* dysregulated in placentas of SCNT-derived offspring.
296
297 As maternal EED is also required for regulating X-inactivation in pre-implantation embryos,
298 and loss of EED in oocytes caused a male bias in fetal lethality in *Eed HET-hom* offspring (Fig.
299 1H)(23, 29), dysregulated X-inactivation may provide another explanation for the gene
300 dysregulation detected in *Eed HET-hom* placenta. To determine if gene expression from the
301 X-chromosome was preferentially impacted in *HET-hom* placentas, we examined the
302 representation of the placental DEGs on all autosomes and the X-chromosome. Placental
303 DEGs with increased expression occurred at a similar rate on the X-chromosome and
304 autosomes, indicating that there was no preferential chromosome-wide de-repression of X-
305 linked genes (Fig. 6C). However, we did note upregulation of X-linked genes *Plac1* and *Ldoc1,*
306 and the imprinted genes *Ascl2* and *Peg3*, which are all known to regulate placental glycogen
307 stores (34) (Supp Fig. 5A). All were increased in the junctional zone DEG list and have been
308 associated with similar placental phenotypes to that observed in here *Eed Het-hom* placentas
309 (Supp Fig. 5A) (39-44). In line with its increased transcription, PLAC1 protein was also
310 increased in cells within the junctional zone (Fig. 6D).
311
312 Finally, we compared *HET-hom* growth patterns with available weight data reported for
313 SCNT-derived offspring, in which H3K27me3 imprinting is disrupted (27). As for *Eed HET-hom*
314 offspring, SCNT-derived offspring were underweight at E14.5, but had caught up by birth
315 (Supp Fig. 6A-B), demonstrating that the growth profiles and placental phenotypes in these
316 models are similar.
317
318 **Discussion**
319 Independent studies have demonstrated that deletion of *Eed* in mouse oocytes using *Zp3Cre*
320 or *Gdf9Cre* results in early growth restriction and offspring overgrowth outcomes in C57BL6
321 mice (7, 23). This study provides a cohesive explanation for these differing reports. We
322 observed time-dependent and inter-related fetal and placental growth trajectories of
323 offspring from *Eed-null* oocytes. Deletion of *Eed* in the oocyte initially led to embryonic and
324 fetal developmental delay, followed by pronounced placental expansion and subsequent
325 rapid catch-up and over-growth of the offspring realised in the early postnatal period.

326

327 Fetal growth restriction is commonly caused by placental insufficiency and is often
328 investigated using surgical or nutritional interventions in animal models (45-49). In this study
329 we provide an intervention that involves only the deletion of *Eed* in the oocyte and in which
330 *HET-hom* offspring were compared to genetically identical *HET-het* controls. We detail fetal
331 growth restriction immediately prior to placental expansion, indicating a role for the placenta
332 in responding to fetal growth restriction to drive offspring catch-up growth prior to birth.
333 Importantly, placental efficiency increased late in gestation and placental hyperplasia
334 immediately preceded the catch-up growth observed in *HET-hom* offspring. Similar outcomes
335 were common between at least two models – the *Eed* oocyte deletion model described here
336 and an SCNT model in which we found published data indicating similar growth restriction
337 occurred prior to placental hyperplasia and subsequent fetal catchup growth was evident.
338 Therefore, in both models, and potentially in others, the data support a model in which initial
339 growth restriction can be corrected by placental expansion at later stages. An imperative for
340 offspring survival is for the delivery of sufficiently developed offspring. Considering this, an
341 interesting conjecture may be that an unknown physiological mechanism detects fetal growth
342 restriction, causing the placenta to respond and mediate intrauterine catch-up growth,
343 potentially rescuing the pregnancy. While speculative, such a mechanism could involve
344 epigenetic adaptation, perhaps H3K27me3-dependent or classical imprinting.

345

346 We observed that the fetal growth restriction, placental hyperplasia and subsequent offspring
347 overgrowth in *Eed HET-hom* offspring was similar to that evident in SCNT-derived offspring.
348 This indicates that the growth patterns for offspring from *Eed*-null oocytes and SCNT are
349 similar. While both models involve loss of H3K27me3-dependent imprinting (23, 26, 27), the
350 SCNT embryos are different to offspring from *Eed*-null oocytes because they were derived
351 from oocytes containing functional maternal PRC2. This might indicate that altered
352 H3K27me3-dependent epigenetic patterning of the oocyte genome is responsible for the
353 early developmental delay in these offspring. However, the underlying cause could differ.
354 SCNT embryos are derived by oocyte-driven reprogramming of a differentiated somatic
355 nucleus, a process through which major epigenetic barriers must be overcome and which may
356 compromise preimplantation development, particularly given that the embryos are
357 transferred to recipient female mice (26, 50-52). Similarly, either loss of maternal PRC2 or

358 H3K27me3 programming caused by *Eed* deletion in the oocyte could explain the reduced
359 blastocyst cell content, and this may underlie early embryo and fetal growth restriction. One
360 way to separate these issues may be to perform pronuclear transfer from *Eed-null* oocytes to
361 wild type oocytes to rescue maternal PRC2 in offspring, and vice versa.
362
363 Comparison of isogenic *HET-hom* and *HET-het* offspring demonstrated that the phenotypic
364 outcomes in this model originate from loss of EED in the oocyte and were largely unaffected
365 by offspring genotype. While *HET-het* offspring maintained normal fetal growth, placental
366 development, gestational length, and litter size, all these aspects of development were
367 substantially modified in isogenic *HET-hom* controls. Other studies have reported that pre-
368 implantation development proceeds normally in offspring from *Eed-null* oocytes, in that
369 blastocysts formed at similar rates and were not affected by increased cell death (23).
370 However, we found that blastocysts derived from *Eed-null* oocytes contained low cell
371 numbers, and that this primarily affected the inner cell mass. Consistent with this, we
372 observed substantial developmental delay in E9.5-E17.5 *HET-hom* offspring derived from *Eed-*
373 *hom* oocytes, but this was resolved by birth and perinatal offspring were ultimately larger
374 than controls.
375
376 There are at least two likely explanations for the early developmental delay observed in this
377 model. EED supplied in the mature oocyte is rapidly localised to the maternal and paternal
378 pronuclei within the first few hours following fertilisation (23, 29, 53, 54) (Jarred et al 2022,
379 submitted). As the *HET-hom* offspring derived from *Eed-null* oocytes lacked maternal EED, it
380 is possible that the lower cell numbers observed at the blastocyst stage resulted from low cell
381 proliferation during pre-implantation development due to a lack of maternally-derived PRC2.
382 This is consistent with the established role for PRC2 in driving cell division in stem cells and
383 other cell types (55) and with a previous report that apoptosis was not increased in blastocysts
384 from EED-null oocytes (23). Alternatively, the lower blastocyst cell counts we observed may
385 have resulted from loss of EED-dependent epigenetic programming in growing oocytes. This
386 programming occurs during a transient stage of PRC2 expression in primary-secondary stage
387 follicles prior to the onset of DNA methylation (22, 56) (Jarred et al 2022, submitted).
388

389 We observed widespread morphological changes in *HET-hom* placental tissue, which
390 presumably provides the required support for late-gestational offspring catch-up growth.
391 Importantly, placental expansion was observed in both fetally- and maternally-derived
392 placental layers, indicating that while placental hyperplasia may be driven through the
393 spongiotrophoblast cells in the junctional layer, the maternal side of the placenta also
394 expands to accommodate greater placental function. Despite this, there was a
395 disproportionate increase in size of the fetally-derived junctional zone compared to the
396 maternally-derived decidual layer. Furthermore, closer examination of the enlarged
397 junctional zone revealed an increase in glycogen enriched cells. This was unusual as glycogen-
398 enriched trophoblasts peak in number at E16.5, but then decline by approximately 60% by
399 E18.5 (34), an outcome reflected in the decreased placental weights we observed in E17.5
400 control offspring. It seems likely that the sustained high levels of glycogen stores in the E17.5
401 placentas of *HET-hom* offspring increase glycogen release to the embryo and drive rapid
402 growth catch-up growth. Glycogen stores in placenta have been proposed to drive fetal
403 growth in other models, however a role for placental conversion of glycogen to glucose for
404 driving fetal catch-up growth is yet to be definitively demonstrated (34). Such a mechanism
405 may act in concert with increased amino acid transport potentially driven by *Slc38a4*, an
406 observation made in SCNT-derived placental hyperplasia (27).
407
408 While fetal growth catch-up is likely to be beneficial for the chances of successful delivery of
409 live offspring, there may be a price to pay for this developmental change in the placenta. In
410 addition to facilitating increased glucose release and rapid fetal catchup growth, glycogen-
411 producing trophoblasts are also considered to facilitate hormonal release from the placenta
412 to the maternal blood supply to prepare the mother for parturition (34, 39). It may be that
413 the increased number of glycogen cells remaining in the late-gestation *HET-hom* placenta
414 delays late gestational hormonal release from the placenta and prolongs pregnancy.
415 Consistent with this, extended gestational length occurred in about two thirds of the
416 pregnancies from *Eed-hom* oocytes. Moreover, while all pups were naturally born, with no
417 apparent birthing difficulties for the mothers, the extended gestational length observed was
418 also associated with very high pup mortality in pregnancies extended by one day and
419 mortality of all offspring in pregnancies extended by two days. While the mechanisms

420 underlying this extended gestation remain obscure, they may have broader implications for
421 understanding the impacts of fetal growth changes on pregnancy outcomes.
422
423 In addition to the morphological alterations observed, we found extensive transcriptional
424 dysregulation in *HET-hom* placentas, with 2083 genes differentially expressed compared to
425 genetically identical *HET-het* placentas. This altered gene expression was not isolated to a
426 single region of the *HET-hom* placenta and was observed in both fetal and maternal layers.
427 While one might expect oocyte-specific loss of EED to affect only fetally-derived placental
428 tissue, this ignores the possibility that the maternal tissue may expand or be re-modelled in
429 response to placental hyperplasia in fetally-derived layers – indeed, without maternal re-
430 modelling it seems likely that the placenta would not properly increase function and support
431 fetal catch-up growth. On this basis, it is unsurprising that transcription was substantially
432 altered in both fetally- and maternally-derived placental tissues.
433
434 Analyses of *HET-hom* placentas identified cellular and morphological changes in maternally-
435 and fetally-derived tissues and placental DEGs that function in multiple systems. Recent work
436 has demonstrated that loss of H3K27me3-dependent imprinting at *Slc38a4* or *Sfmbt2,* and to
437 a lesser extent, *Gab1* or *Smoc1,* leads to placental hyperplasia in SCNT-derived offspring (25-
438 27, 57). Consistent with this, we observed placental hyperplasia and increased expression of
439 *Slc38a4, Sfmbt2, Gab1 and Smoc1* in placentas from *Eed-null* oocytes, suggesting a loss of
440 H3K27me3-dependent imprinting at these genes. We also observed increased placental
441 expression of the X-linked genes *Plac1*, *Wdr1* and *Ldoc1,* and immunohistochemistry
442 confirmed that PLAC1 expression was increased in junctional zone cells in *HET-hom* placentas.
443 However, deletion of *Plac1*, rather than increased expression, has been associated with a
444 similar placental phenotype and male biased lethality to that observed in *HET-hom* offspring
445 (58). Notwithstanding this difference, it seems likely that the fetal growth restriction,
446 placental hyperplasia, and fetal catch-up growth in this model involves one or all of these
447 genes. Substantial additional work is required to understand the mechanisms involved and
448 the interactions between the genes that contribute.
449
450 While we observed no difference in the number of surviving hatched or expanded blastocysts
451 from *Eed-hom* mothers, there was a decrease in the blastocyst cell count, particularly in the

452 ICM, and a marked decrease in *HET-hom* litter size. Consistent with this and with another
453 study (23), we also observed smaller offspring at E9.5, developmental delay and loss of
454 embryos by E12.5, and reduced litter size at term (7). While the reason for *HET-hom* offspring
455 loss is yet to be identified, one possibility is that the significant reduction in blastocyst cell
456 numbers and subsequent developmental delay is too profound to support survival during
457 mid-gestation development in the most highly impacted offspring. This may involve impacts
458 within the embryo itself, and/or contributions from a defective placenta. The placenta
459 develops a capacity to exchange nutrients, other supportive metabolites, and waste between
460 the maternal and fetal blood supply at E9.5, and increased embryo loss around this stage
461 could indicate early-mid gestational placental insufficiency (59, 60). Embryonic lethality has
462 also been previously linked to placental defects in knockout studies of imprinted and X-linked
463 genes *Plac1*, *Ascl2* and *Peg10* (39-41, 43, 44, 61). As *Plac1* and *Ascl2* transcription was
464 increased in the late-gestation *HET-hom* placenta, altered expression of imprinted genes such
465 as *Plac1* or *Ascl2* may contribute to placental defects and fetal death in this model.
466
467 In summary, we demonstrate that loss of PRC2 function in the oocyte profoundly affects
468 growth and developmental outcomes in both offspring and placenta via a mechanism that is
469 independent of genetic background. This involves initial embryonic developmental delay and
470 fetal growth restriction, followed by remarkable placental expansion, increased placental
471 glycogen stores and fetal catch-up growth (Fig 7). These outcomes were associated with
472 increased expression of genes associated with placental hyperplasia. Importantly, rapid fetal
473 growth restriction and fetal catch-up growth have been linked with negative health outcomes
474 later in life, including metabolic conditions (62, 63). Moreover, given that mutations in the
475 core PRC2 genes, EED, EZH2 and SUZ12 have all been associated with overgrowth and a range
476 of co-morbidities in Cohen-Gibson, Weaver and Imagawa-Matsumoto syndrome patients (14,
477 15, 17, 19, 20) and we have observed similarities in outcomes of mouse offspring lacking EED
478 in oocytes (7) this work also has implications for understanding these rare conditions.
479 Together, this research reveals that altered PRC2-dependent programming in the oocyte
480 elicits a complex intrauterine environment for the fetus, which has the potential to mediate
481 impacts on offspring health and disease that may persist into adulthood.

482 **Methods**

483 **Mouse strains, animal care and ethics**

484 Mice were housed using a 12h light-dark cycle at Monash Medical Centre Animal Facility, as
485 previously reported (7). Room temperature was maintained at 21-23°C with controlled
486 humidity, and food and water were provided *ad libitum*. All animal work was undertaken in
487 accordance with Monash University Animal Ethics Committee (AEC) approval. Mice were
488 obtained from the following sources: *Zp3Cre* mice (C57BL/6-Tg 93knw/J; Jackson Labs line
489 003651, constructed and shared by Prof Barbara Knowles(64), *Eed* floxed mice (*Eed*$^{fl/fl}$) (B6;
490 129S1-*Eed*tm1Sho/J; Jackson Labs line 0022727; constructed and shared by Prof Stuart Orkin
491 (65). The *Eed* line was backcrossed to a pure C57BL6/J and shared with us by Associate
492 Professor Rhys Allen and Professor Marnie Blewitt, Walter and Eliza Hall Institute for Medical
493 Research, Melbourne.

494

495 **Genotyping**

496 Genotyping was performed by Transnetyx (Cordova, TN) using real-time PCR assays (details
497 available upon request) designed for each gene as described previously (7).

498

499 **Collection and culture of pre-implantation embryos**

500 Eight to twelve-week-old female mice were superovulated and mated to C57BL/6 males for
501 one night. Zygotes were collected in handling media (G-MOPS PLUS, Vitrolife) at 37°C (28, 66)
502 denuded of cumulus cells with G-MOPS PLUS containing hyaluronidase. All embryos were
503 washed in G-MOPS PLUS and embryo development kinetics was assessed using the
504 EmbryoScope™ (Vitrolife) time-lapse imaging system. Embryos were cultured individually in
505 25µl of medium, with time-lapse images generated at 15-minute (min) intervals throughout
506 the culture period.

507

508 **Cell allocation in blastocysts**

509 Following EmbryoScope™ culture, differential staining was performed (67) in hatched
510 blastocysts using propidium iodide to label TE nuclei, while leaving the ICM unlabelled. After
511 fixation, embryos were treated with bisbenzimide to stain ICM and TE, whole-mounted in
512 glycerol and imaged using an inverted fluorescence microscope (Nikon Eclipse TS100). Nuclei
513 were counted using ImageJ.

514

515 **Collection of post-implantation embryos, placenta and postnatal offspring**

516 Mice were time mated for two-four nights, with females plug checked daily. Positive plugs
517 were noted as day E0.5. Pregnant females were euthanised and embryos collected at E9.5,
518 E12.5 E14.5 and E17.5. E9.5 whole sacs were weighed, fixed in 4% PFA for 72h at 4°C degrees
519 processed, paraffin embedded, sectioned at 5µm. Whole-mount images of E9.5 embryos
520 were taken using a LEICA M80 light microscope with LEICA MC170 HD camera
521 attachment. E12.5, E14.5 and E17.5 embryos and placentas were isolated and weighed.
522 Placentas were then bisected, and half was fixed in 4% PFA for 72h at 4°C degrees, processed
523 and paraffin embedded. The other half of the placenta was rinsed in PBS, snap-frozen on dry
524 ice and stored at -80°C for RNA analysis. P0 and P3 offspring were weighed and euthanized
525 by decapitation. All offspring samples were collected from at least three different females /
526 genotype.

527

528 **Placental Histology**

529 Paraffin embedded placentas were sectioned at 5µm using a Leica microtome and sections
530 transferred to Superfrost plus slides (Thermo-Fisher, Braunschweig, Germany). Periodic
531 antigen-shiff (PAS) and hematoxylin and eosin (H&E) staining was performed on placental
532 sections by the Monash Histology Platform (MHTP node). Stained slides were scanned using
533 Aperio slide scanner by the Monash Histology Platform and analysis was conducted using
534 QuPath v0.2.3[42]. Junctional zone, labyrinth and decidual area was calculated in E14.5 and
535 E17.5 H&E stained placentas. Glycogen cell counts were also conducted on H&E stained E14.5
536 and E17.5 placentas using QuPath v0.2.3[42]. Investigators were blinded for sample genotypes
537 throughout quantitative scoring of placental samples analysed.

538

539 **Immunohistochemistry**

540 Slides with 5µm thick placental sections were baked at 60°C for 20 mins. Tissue sections were
541 dewaxed in three changes of xylene and rehydrated in three changes of ethanol then rinsed
542 in distilled water. Antigen retrieval was performed in DAKO PT Link in a DAKO Target Retrieval
543 (Low pH) Solution (DAKO, Cat# S1699) at 98°C for 30 min. Slides were then washed in DAKO
544 EnVision Flex Wash Buffer (Cat# K8000) for 5 minutes. IHC was then performed on a DAKO
545 Autostainer Plus in the following steps. Sections were washed once in EnVision Flex Wash

546 Buffer following each subsequent step. Peroxidase Blocking Solution (DAKO, Cat# S2023) was
547 applied for 10 minutes and non-specific binding was prevented with AffiniPure Fab Fragment
548 Goat Anti-Mouse IgG for 1 hour. Mouse anti-PLAC1 (G-1) (Santa Cruz, Cat# sc-365919) primary
549 antibody was applied at an appropriate concentration for 1 hour. EnVision System-HRP
550 Labelled Polymer Anti-Mouse (DAKO, Cat# K4001) was applied for 1 hour. Immunostaining
551 was visualised using DAKO Liquid DAB+ Substrate Chromogen System (Cat# K3468). A
552 counterstain DAKO Automation Haematoxylin Staining Reagent was then applied for 10
553 minutes. Slides were removed from the Autostainer, transferred to a slide staining rack and
554 rinsed in distilled water. In a fume-hood, slides were then washed in Scott's Tap water and
555 distilled water. Finally, slides were dehydrated in three changes of 100% Ethanol, cleared in
556 three changes of Xylene and mounted in DPX. Slides were either scanned using a VS120
557 Slidescanner (Olympus).
558
559 **Placental RNA-sequencing**
560 Placental isolation is described above, and placental RNA was extracted from 4-5
561 samples/genotype using NucleoSpin RNA Plus columns. RNA quality was assessed on an
562 Agilent Bioanalyser and samples with RIN >7.5 used for library preparation and sequencing
563 on the BGI Genomics platform (BGI Genomics, Hong Kong).
564
565 **Statistical Analyses**
566 Statistical analyses were performed using GraphPad Prism according to the statistical triage
567 provided in the package. In brief, for parametric tests one way ANOVA with multiple
568 comparison testing was used, with Student's *t* tests for pairwise comparisons included. If
569 indicated in GraphPad Prism, non-parametric were applied. Tests used are indicated in
570 figure legends.
571
572 **RNA-sequencing data analyses**
573 Adaptor and low-quality sequences in raw sequencing reads were trimmed using
574 Trimmomatic (68) (v0.39) with the following parameters: LEADING:3 TRAILING:3
575 SLIDINGWINDOW:4:15 MINLEN:20. Clean reads were mapped to the mouse reference
576 genome (GRCm38) using STAR (v2.7.5c) with the following settings:
577 outFilterMismatchNoverLmax 0.03 --alignIntronMax 10000. Raw counts for mouse reference

genes (ensembl-release-101) were calculated using STAR (v2.7.5c) with parameter "--quantMode GeneCounts" simultaneously when doing the genome mapping. Differential gene expression analysis was carried out using the R package "limma" (69) with "treat" function and parameter "lfc=log(1.1)". Statistically significantly differentially expressed genes were identified using "FDR < 0.05". Gene Ontology (GO) enrichment analysis for significantly differentially expressed genes was carried out using The Database for Annotation, Visualisation and Integrated Discovery (DAVID) with following settings: GO term level 3, minimum gene count 5, and FDR < 0.05 (70).

Declarations

Acknowledgments:
We thank Dr. Neil Youngson and Prof. Marnie Blewitt for critical comments on the manuscript, Monash Animal Research Platform staff for assistance with mouse care, Monash Histology Platform for assistance with slide scanning and the Monash Micro Imaging Facility and MHTP Medical Genomics Facilities for assistance and technical advice.

Ethics approvals:
All animal work was undertaken in accordance with Monash University Animal Ethics Committee (AEC) approval.

Availability of data and materials
All RNA sequencing data have been deposited to the Gene Expression Omnibus (GEO) and are publicly available with accession number GSE210398. All other information is available from the corresponding author.

Competing interests:
The authors declare that they have no competing interests that affect this work

Funding:
This work was supported by grants and research funding from:
National Health and Medical Research Project Grant GNT1144966 (PSW, DKG, MvdB, DLA)
Hudson Institute of Medical Research (PSW)
Victorian Government's Operational Infrastructure Support Program.
Australian Government Research Training Program Scholarship (EGJ, RO and SP)

Author contributions:
Conceived and/or designed experiments: RO, SP, TT, ZQ, EJ, HB, PSW
Performed experiments and/or analysed data: RO, SP, TT, TTT, DF, ZQ, EJ, HB, PSW
Bioinformatic analyses and/or comparisons with published datasets: ZQ, RO, SP, DLA, PSW
Resources and/or supervision PSW DKG, MvdB, DLA, NAS
Writing - original draft: RO, SP, PSW

Writing - review & editing: RO, SP, EJ, PSW, NAS. All authors critically read and approved the manuscript.

References

1. Maccani MA, Marsit CJ. Epigenetics in the placenta. *Am J Reprod Immunol.* 2009;62(2):78-89.
2. Sun L, Fu X, Ma G, Hutchins AP. Chromatin and Epigenetic Rearrangements in Embryonic Stem Cell Fate Transitions. *Front Cell Dev Biol.* 2021;9:637309.
3. Pasini D, Bracken AP, Jensen MR, Denchi EL, Helin K. Suz12 is essential for mouse development and for EZH2 histone methyltransferase activity. *Embo J.* 2004;23(20):4061-71.
4. Faust C, Schumacher A, Holdener B, Magnuson T. The eed mutation disrupts anterior mesoderm production in mice. *Development.* 1995;121(2):273-85.
5. O'Carroll D, Erhardt S, Pagani M, Barton SC, Surani MA, Jenuwein T. The polycomb-group gene Ezh2 is required for early mouse development. *Mol Cell Biol.* 2001;21:4330-6.
6. Shen X, Liu Y, Hsu YJ, Fujiwara Y, Kim J, Mao X, Yuan GC, Orkin SH. EZH1 mediates methylation on histone H3 lysine 27 and complements EZH2 in maintaining stem cell identity and executing pluripotency. *Mol Cell.* 2008;32(4):491-502.
7. Prokopuk L, Stringer JM, White CR, Vossen RHAM, White SJ, Cohen ASA, Gibson WT, Western PS. Loss of maternal EED results in postnatal overgrowth. *Clin Epigenetics.* 2018;10(1).
8. Boyer LA, Plath K, Zeitlinger J, Brambrink T, Medeiros LA, Lee TI, Levine SS, Wernig M, Tajonar A, Ray MK, Bell GW, Otte AP, Vidal M, Gifford DK, Young RA, Jaenisch R. Polycomb complexes repress developmental regulators in murine embryonic stem cells. *Nature.* 2006;441(7091):349-53.
9. Hemming S, Cakouros D, Isenmann S, Cooper L, Menicanin D, Zannettino A, Gronthos S. EZH2 and KDM6A Act as an Epigenetic Switch to Regulate Mesenchymal Stem Cell Lineage Specification. *Stem Cells.* 2014;32(3):802-15.
10. Dudakovic A, Camilleri ET, Xu F, Riester SM, McGee-Lawrence ME, Bradley EW, Paradise CR, Lewallen EA, Thaler R, Deyle DR, Larson AN, Lewallen DG, Dietz AB, Stein GS, Montecino MA, Westendorf JJ, van Wijnen AJ. Epigenetic Control of Skeletal Development by the Histone Methyltransferase Ezh2. *J Biol Chem.* 2015;290(46):27604.
11. Majewski IJ, Ritchie ME, Phipson B, Corbin J, Pakusch M, Ebert A, Busslinger M, Koseki H, Hu Y, Smyth GK, Alexander WS, Hilton DJ, Blewitt ME. Opposing roles of polycomb repressive complexes in hematopoietic stem and progenitor cells. *Blood.* 2010;116(5):731-9.
12. Liu PP, Xu YJ, Dai SK, Du HZ, Wang YY, Li XG, Teng ZQ, Liu CM. Polycomb Protein EED Regulates Neuronal Differentiation through Targeting SOX11 in Hippocampal Dentate Gyrus. *Stem Cell Rep.* 2019;13(1):115-31.
13. Sun B, Chang E, Gerhartl A, Szele FG. Polycomb Protein Eed is Required for Neurogenesis and Cortical Injury Activation in the Subventricular Zone. *Cerebral Cortex.* 2018;28(4):1369-82.
14. Cohen AS, Gibson WT. EED-associated overgrowth in a second male patient. *J Hum Genet.* 2016;61(9):831-4.

15. Tatton-Brown K, Hanks S, Ruark E, Zachariou A, Duarte Sdel V, Ramsay E, Snape K, Murray A, Perdeaux ER, Seal S, Loveday C, Banka S, Clericuzio C, Flinter F, Magee A, McConnell V, Patton M, Raith W, Rankin J, Splitt M, Strenger V, Taylor C, Wheeler P, Temple KI, Cole T, Childhood Overgrowth C, Douglas J, Rahman N. Germline mutations in the oncogene EZH2 cause Weaver syndrome and increased human height. *Oncotarget.* 2011;2(12):1127-33.
16. Cohen AS, Yap DB, Lewis ME, Chijiwa C, Ramos-Arroyo MA, Tkachenko N, Milano V, Fradin M, McKinnon ML, Townsend KN, Xu J, Van Allen MI, Ross CJ, Dobyns WB, Weaver DD, Gibson WT. Weaver Syndrome-Associated EZH2 Protein Variants Show Impaired Histone Methyltransferase Function In Vitro. *Hum Mutat.* 2016;37(3):301-7.
17. Cooney E, Bi W, Schlesinger AE, Vinson S, Potocki L. Novel EED mutation in patient with Weaver syndrome. *Am J Med Genet.* 2017;173(2):541-5.
18. Imagawa E, Higashimoto K, Sakai Y, Numakura C, Okamoto N, Matsunaga S, Ryo A, Sato Y, Sanefuji M, Ihara K, Takada Y, Nishimura G, Saitsu H, Mizuguchi T, Miyatake S, Nakashima M, Miyake N, Soejima H, Matsumoto N. Mutations in genes encoding polycomb repressive complex 2 subunits cause Weaver syndrome. *Hum Mutat.* 2017;38(6):637-48.
19. Imagawa E, Albuquerque EVA, Isidor B, Mitsuhashi S, Mizuguchi T, Miyatake S, Takata A, Miyake N, Boguszewski MCS, Boguszewski CL, Lerario AM, Funari MA, Jorge AAL, Matsumoto N. Novel SUZ12 mutations in Weaver-like syndrome. *Clin Genet.* 2018;94(5):461-6.
20. Tatton-Brown K, Murray A, Hanks S, Douglas J, Armstrong R, Banka S, Bird LM, Clericuzio CL, Cormier-Daire V, Cushing T, Flinter F, Jacquemont M-L, Joss S, Kinning E, Lynch SA, Magee A, McConnell V, Medeira A, Ozono K, Patton M, Rankin J, Shears D, Simon M, Splitt M, Strenger V, Stuurman K, Taylor C, Titheradge H, Van Maldergem L, Temple IK, Cole T, Seal S, Consortium CO, Rahman N. Weaver syndrome and EZH2 mutations: Clarifying the clinical phenotype. *Am J MedGenet.* 2013;161(12):2972-80.
21. Hanna CW, Kelsey G. Features and mechanisms of canonical and noncanonical genomic imprinting. *Genes Dev.* 2021;35(11-12):821-34.
22. Inoue A, Jiang L, Lu F, Suzuki T, Zhang Y. Maternal H3K27me3 controls DNA methylation-independent imprinting. *Nature.* 2017;547(7664).
23. Inoue A, Chen Z, Yin Q, Zhang Y. Maternal Eed knockout causes loss of H3K27me3 imprinting and random X inactivation in the extraembryonic cells. *Genes Dev.* 2018;32(23-24):1525-36.
24. Matoba S, Wang H, Jiang L, Lu F, Iwabuchi KA, Wu X, Inoue K, Yang L, Press W, Lee JT, Ogura A, Shen L, Zhang Y. Loss of H3K27me3 Imprinting in Somatic Cell Nuclear Transfer Embryos Disrupts Post-Implantation Development. *Cell Stem Cell.* 2018;23(3):343-54.e5.
25. Inoue K, Ogonuki N, Kamimura S, Inoue H, Matoba S, Hirose M, Honda A, Miura K, Hada M, Hasegawa A, Watanabe N, Dodo Y, Mochida K, Ogura A. Loss of H3K27me3 imprinting in the Sfmbt2 miRNA cluster causes enlargement of cloned mouse placentas. *Nat Commun.* 2020;11(1):2150.
26. Wang L-Y, Li Z-K, Wang L-B, Liu C, Sun X-H, Feng G-H, Wang J-Q, Li Y-F, Qiao L-Y, Nie H, Jiang L-Y, Sun H, Xie Y-L, Ma S-N, Wan H-F, Lu F-L, Li W, Zhou Q. Overcoming Intrinsic H3K27me3 Imprinting Barriers Improves Post-implantation Development after Somatic Cell Nuclear Transfer. *Cell Stem Cell.* 2020;27(2):315-25.e5.

711 27. Xie Z, Zhang W, Zhang Y. Loss of Slc38a4 imprinting is a major cause of mouse placenta
712 hyperplasia in somatic cell nuclear transferred embryos at late gestation. *Cell Rep.*
713 2022;38(8):110407-.
714 28. Gardner DK, Lane M. Mammalian Preimplantation Embryo Culture. In: Lewandoski M,
715 editor. *Mouse Molecular Embryology: Methods and Protocols.* Boston, MA: Springer US;
716 2014. p. 167-82.
717 29. Harris C, Cloutier M, Trotter M, Hinten M, Gayen S, Du Z, Xie W, Kalantry S. Conversion
718 of random X-inactivation to imprinted X-inactivation by maternal PRC2. *eLife.*
719 2019;8:e44258.
720 30. Krombeen SK, Shankar V, Noorai RE, Saski CA, Sharp JL, Wilson ME, Wilmoth TA. The
721 identification of differentially expressed genes between extremes of placental
722 efficiency in maternal line gilts on day 95 of gestation. *BMC Genom.* 2019;20(1):254.
723 31. Coan PM, Conroy N, Burton GJ, Ferguson-Smith AC. Origin and characteristics of
724 glycogen cells in the developing murine placenta. *Dev Dyn.* 2006;235(12):3280-94.
725 32. McLellan AS, Fischer B, Dveksler G, Hori T, Wynne F, Ball M, Okumura K, Moore T,
726 Zimmermann W. Structure and evolution of the mouse pregnancy-specific glycoprotein
727 (Psg) gene locus. *BMC Genom.* 2005;6(1):4.
728 33. Simmons DG, Rawn S, Davies A, Hughes M, Cross JC. Spatial and temporal expression of
729 the 23 murine Prolactin/Placental Lactogen-related genes is not associated with their
730 position in the locus. *BMC Genom.* 2008;9(1):352.
731 34. Tunster SJ, Watson ED, Fowden AL, Burton GJ. Placental glycogen stores and fetal
732 growth: insights from genetic mouse models. *Reproduction.* 2020;159(6):R213-R35.
733 35. Han X, Wang R, Zhou Y, Fei L, Sun H, Lai S, Saadatpour A, Zhou Z, Chen H, Ye F, Huang D,
734 Xu Y, Huang W, Jiang M, Jiang X, Mao J, Chen Y, Lu C, Xie J, Fang Q, Wang Y, Yue R, Li T,
735 Huang H, Orkin SH, Yuan G-C, Chen M, Guo G. Mapping the Mouse Cell Atlas by
736 Microwell-Seq. *Cell.* 2018;173(5):1307-.
737 36. Woods L, Perez-Garcia V, Hemberger M. Regulation of Placental Development and Its
738 Impact on Fetal Growth—New Insights From Mouse Models. *Front Endocrinol.* 2018;9.
739 37. Andergassen D, Dotter CP, Wenzel D, Sigl V, Bammer PC, Muckenhuber M, Mayer D,
740 Kulinski TM, Theussl H-C, Penninger JM, Bock C, Barlow DP, Pauler FM, Hudson QJ.
741 Mapping the mouse Allelome reveals tissue-specific regulation of allelic expression.
742 *Elife.* 2017;6.
743 38. Wanigasuriya I, Gouil Q, Kinkel SA, del Fierro AT, Beck T, Roper EA, Breslin K, Stringer J,
744 Hutt K, Lee HJ, Keniry A, Ritchie ME, Blewitt ME. Smchd1 is a maternal effect gene
745 required for genomic imprinting. *Elife.* 2020;9.
746 39. Tunster SJ, McNamara GI, Creeth HDJ, John RM. Increased dosage of the imprinted Ascl2
747 gene restrains two key endocrine lineages of the mouse Placenta. *Dev Biol.*
748 2016;418(1):55-65.
749 40. Tunster SJ, Boqué-Sastre R, McNamara GI, Hunter SM, Creeth HDJ, John RM. Peg3
750 Deficiency Results in Sexually Dimorphic Losses and Gains in the Normal Repertoire of
751 Placental Hormones. *Front Cell Dev Biol.* 2018;6.
752 41. Lee S, Ye A, Kim J. DNA-Binding Motif of the Imprinted Transcription Factor PEG3. *PLoS*
753 *One.* 2015;10(12):e0145531.
754 42. Allas L, Boumédiene K, Baugé C. Epigenetic dynamic during endochondral ossification
755 and articular cartilage development. *Bone.* 2019;120:523-32.
756 43. Thiaville MM, Huang JM, Kim H, Ekram MB, Roh T-Y, Kim J. DNA-binding motif and target
757 genes of the imprinted transcription factor PEG3. *Gene.* 2013;512(2):314-20.

758 44. Naruse M, Ono R, Irie M, Nakamura K, Furuse T, Hino T, Oda K, Kashimura M, Yamada I,
759 Wakana S, Yokoyama M, Ishino F, Kaneko-Ishino T. Sirh7/Ldoc1 knockout mice exhibit
760 placental P4 overproduction and delayed parturition. *Development.*
761 2014;141(24):4763-71.
762 45. Palliser HK, Yates DM, Hirst JJ. Progesterone Receptor Isoform Expression in Response
763 to in utero Growth Restriction in the Fetal Guinea Pig Brain. *Neuroendocrinology.*
764 2012;96(1):60-7.
765 46. Louey S, Cock ML, Stevenson KM, Harding R. Placental insufficiency and fetal growth
766 restriction lead to postnatal hypotension and altered postnatal growth in sheep. *Pediatr*
767 *Res.* 2000;48(6):808-14.
768 47. Supramaniam V, Jenkin G, Loose J, Wallace E, Miller S. Basic science: Chronic fetal
769 hypoxia increases activin A concentrations in the late-pregnant sheep. *BJOG - Int J Obst*
770 *Gy.* 2006;113(1):102-9.
771 48. Swanson AM, David AL. Animal models of fetal growth restriction: Considerations for
772 translational medicine. *Placenta.* 2015;36(6):623-30.
773 49. Vuguin PM. Animal Models for Small for Gestational Age and Fetal Programing of Adult
774 Disease. *Horm Res Paediatr.* 2007;68(3):113-23.
775 50. Matoba S, Liu Y, Lu F, Iwabuchi Kumiko A, Shen L, Inoue A, Zhang Y. Embryonic
776 Development following Somatic Cell Nuclear Transfer Impeded by Persisting Histone
777 Methylation. *Cell.* 2014;159(4):884-95.
778 51. Liu W, Liu X, Wang C, Gao Y, Gao R, Kou X, Zhao Y, Li J, Wu Y, Xiu W, Wang S, Yin J, Liu
779 W, Cai T, Wang H, Zhang Y, Gao S. Identification of key factors conquering
780 developmental arrest of somatic cell cloned embryos by combining embryo biopsy and
781 single-cell sequencing. *Cell Discov. 2*016;2(1):16010.
782 52. Ogura A, Matoba S, Inoue K. Anniversay of Cloning by Somatic-Cell Nuclear Transfer:
783 Epigenetic abnormalities associated with somatic cell nuclear transfer. *Reproduction.*
784 2021;162(1):F45-F58.
785 53. Erhardt S, Su IH, Schneider R, Barton S, Bannister AJ, Perez-Burgos L, Jenuwein T,
786 Kouzarides T, Tarakhovsky A, Surani MA. Consequences of the depletion of zygotic and
787 embryonic enhancer of zeste 2 during preimplantation mouse development.
788 *Development.* 2003;130(18):4235.
789 54. Inoue A, Jiang L, Lu F, Zhang Y. Genomic imprinting of Xist by maternal H3K27me3.
790 *Genes Dev.* 2017;31(19):1927.
791 55. Bracken AP, Pasini D, Capra M, Prosperini E, Colli E, Helin K. EZH2 is downstream of the
792 pRB-E2F pathway, essential for proliferation and amplified in cancer. *Embo J.*
793 2003;22(20):5323-35.
794 56. Zheng H, Huang B, Zhang B, Xiang Y, Du Z, Xu Q, Li Y, Wang Q, Ma J, Peng X, Xu F, Xie W.
795 Resetting Epigenetic Memory by Reprogramming of Histone Modifications in Mammals.
796 *Mol Cell.* 2016;63(6):1066-79.
797 57. Miri K, Latham K, Panning B, Zhong Z, Andersen A, Varmuza S. The imprinted polycomb
798 group gene Sfmbt2 is required for trophoblast maintenance and placenta development.
799 *Development.* 2013;140(22):4480-9.
800 58. Jackman SM, Kong X, Fant ME. Plac1 (placenta-specific 1) is essential for normal
801 placental and embryonic development. *Mol Reprod Dev.* 2012;79(8):564-72.
802 59. Watson ED, Cross JC. Development of Structures and Transport Functions in the Mouse
803 Placenta. *Physiology.* 2005;20(3):180-93.

804 60. Starks RR, Kaur H, Tuteja G. Mapping cis-regulatory elements in the midgestation mouse
805 placenta. *Sci Rep.* 2021;11(1):22331-.
806 61. He H, Perera BPU, Ye A, Kim J. Parental and sexual conflicts over the Peg3 imprinted
807 domain. *Sci Rep.* 2016;6(1):38136.
808 62. Singhal A, Lucas A. Early origins of cardiovascular disease: is there a unifying hypothesis?
809 *The Lancet.* 2004;363(9421):1642-5.
810 63. Singhal A. Long-Term Adverse Effects of Early Growth Acceleration or Catch-Up Growth.
811 *Ann Nutr Metab.* 2017;70(3):236-40.
812 64. de Vries WN, Binns LT, Fancher KS, Dean J, Moore R, Kemler R, Knowles BB. Expression
813 of Cre recombinase in mouse oocytes: a means to study maternal effect genes. *Genesis.*
814 2000;26(2):110-2.
815 65. Yu M, Riva L, Xie H, Schindler Y, Moran TB, Cheng Y, Yu D, Hardison R, Weiss MJ, Orkin
816 SH, Bernstein BE, Fraenkel E, Cantor AB. Insights into GATA-1-mediated gene activation
817 versus repression via genome-wide chromatin occupancy analysis. *Mol Cell.*
818 2009;36(4):682-95.
819 66. Gardner DK, Truong TT. Culture of the Mouse Preimplantation Embryo. *Methods Mol*
820 *Biol.* 2019;2006:13-32.
821 67. Hardy K, Handyside AH, Winston RM. The human blastocyst: cell number, death and
822 allocation during late preimplantation development in vitro. *Development.*
823 1989;107(3):597-604.
824 68. Bolger AM, Lohse M, Usadel B. Trimmomatic: a flexible trimmer for Illumina sequence
825 data. *Bioinformatics.* 2014;30(15):2114-20.
826 69. Ritchie ME, Phipson B, Wu D, Hu Y, Law CW, Shi W, Smyth GK. limma powers differential
827 expression analyses for RNA-sequencing and microarray studies. *Nucleic Acids Res.*
828 2015;43(7):e47-e.
829 70. Dennis G, Jr., Sherman BT, Hosack DA, Yang J, Gao W, Lane HC, Lempicki RA. DAVID:
830 Database for Annotation, Visualization, and Integrated Discovery. *Genome Biol.*
831 2003;4(5):P3.
832

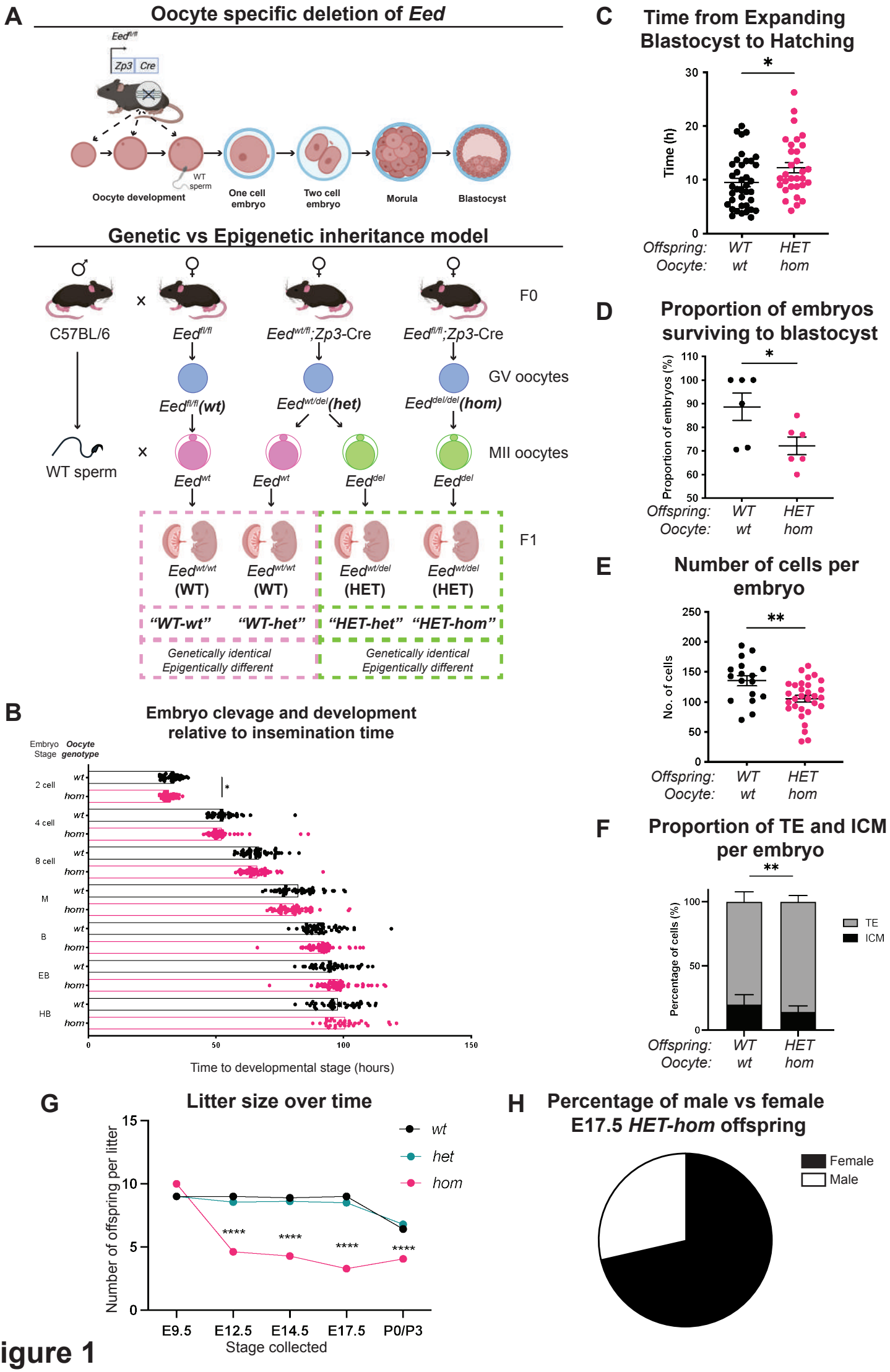
A
Oocyte specific deletion of Eed
Eedfl/fl
Zp3
Cre
WT sperm
Oocyte development
One cell embryo
Two cell embryo
Morula
Blastocyst
Genetic vs Epigenetic inheritance model
C57BL/6
Eedfl/fl
Eedwt/fl;Zp3-Cre
Eedfl/fl;Zp3-Cre
F0
GV oocytes
Eedfl/fl(wt)
Eedwt/del(het)
Eeddel/del(hom)
WT sperm
MII oocytes
Eedwt
Eedwt
Eeddel
Eeddel
F1
Eedwt/wt (WT)
Eedwt/wt (WT)
Eedwt/del (HET)
Eedwt/del (HET)
"WT-wt"
"WT-het"
"HET-het"
"HET-hom"
Genetically identical Epigenetically different
Genetically identical Epigenetically different
B
Embryo clevage and development relative to insemination time
Embryo Stage
Oocyte genotype
2 cell
4 cell
8 cell
M
B
EB
HB
wt
hom
Time to developmental stage (hours)
C
Time from Expanding Blastocyst to Hatching
Time (h)
Offspring: WT HET
Oocyte: wt hom
D
Proportion of embryos surviving to blastocyst
Proportion of embryos (%)
Offspring: WT HET
Oocyte: wt hom
E
Number of cells per embryo
No. of cells
Offspring: WT HET
Oocyte: wt hom
F
Proportion of TE and ICM per embryo
Percentage of cells (%)
TE
ICM
Offspring: WT HET
Oocyte: wt hom
G
Litter size over time
Number of offspring per litter
wt
het
hom
E9.5
E12.5
E14.5
E17.5
P0/P3
Stage collected
H
Percentage of male vs female E17.5 HET-hom offspring
Female
Male

Figure 1

833 **Figure Legends**

834 **Figure 1. Maternal *Eed* deletion impacted pre-implantation development. (a)** Model used to
835 generate heterozygous isogenic offspring from oocytes that lacked or retained *Eed.* Females
836 producing *Eed-wt*, *Eed-het* and *Eed-hom* oocytes were mated with wild type males to produce
837 offspring from oocytes with *wt* or *het* EED-dependent programming or from oocytes that lack
838 EED-dependent programming respectively. *Eed-wt* oocytes produce *WT* offspring (*WT-wt*
839 control), *Eed-het* oocytes produce *WT* or *HET* offspring (*WT-het* and *HET-het*) from the same
840 GV oocyte, and *Eed-hom* oocytes produce *HET* offspring (*HET-hom*). *HET-het* and *HET-hom*
841 offspring are isogenic, but were derived from oocytes that had different EED-dependent
842 programming. **(b)** Cell cleavage and development times of embryos from *Eed-wt* or *Eed-hom*
843 oocytes in *ex vivo* culture. Data is presented as time to reach 2-, 4-, 8-cell, morula (M),
844 blastocyst (B), expanded blastocyst (EB) and hatched blastocyst (HB). *P<0.05, two-tailed
845 student's t test, N = 49 embryos from *Eed-wt* oocytes, 57 embryos from *Eed-hom* oocytes. **(c)**
846 Time taken for expanded blastocysts to hatch. Data represents the time difference between
847 hatched blastocyst and expanded blastocysts. *P<0.05, N = 38 embryos from *Eed-wt* oocytes,
848 31 embryos from *Eed-hom* oocytes. **(d)** Proportion of embryos from *Eed-wt* or *Eed-hom*
849 oocytes surviving to blastocyst. *P<0.05, Data represent the proportion of surviving embryos
850 from each female, N = 6 females. **(e)** Total number of cells per embryo. **P<0.005, N = 17
851 embryos from *Eed-wt* oocytes, 30 embryos from *Eed-hom* oocytes. **(f)** Proportion of TE and
852 ICM cells per embryo. Data represents the mean proportion of cells allocated to TE versus
853 ICM for embryos from *Eed-wt* or *Eed-hom* oocytes. **P<0.05, N = 17 embryos from *Eed-wt*
854 oocytes, 28 embryos from *Eed-hom* oocytes. **(g)** Offspring litter size over time. ****P<0.0001.
855 **(h)** Pie chart depicting the proportion of male and female *HET-hom* offspring at E17.5. N=32.
856 For **(b-g)** a two-tailed student's t test was used and error bars represent mean ± SD.
857

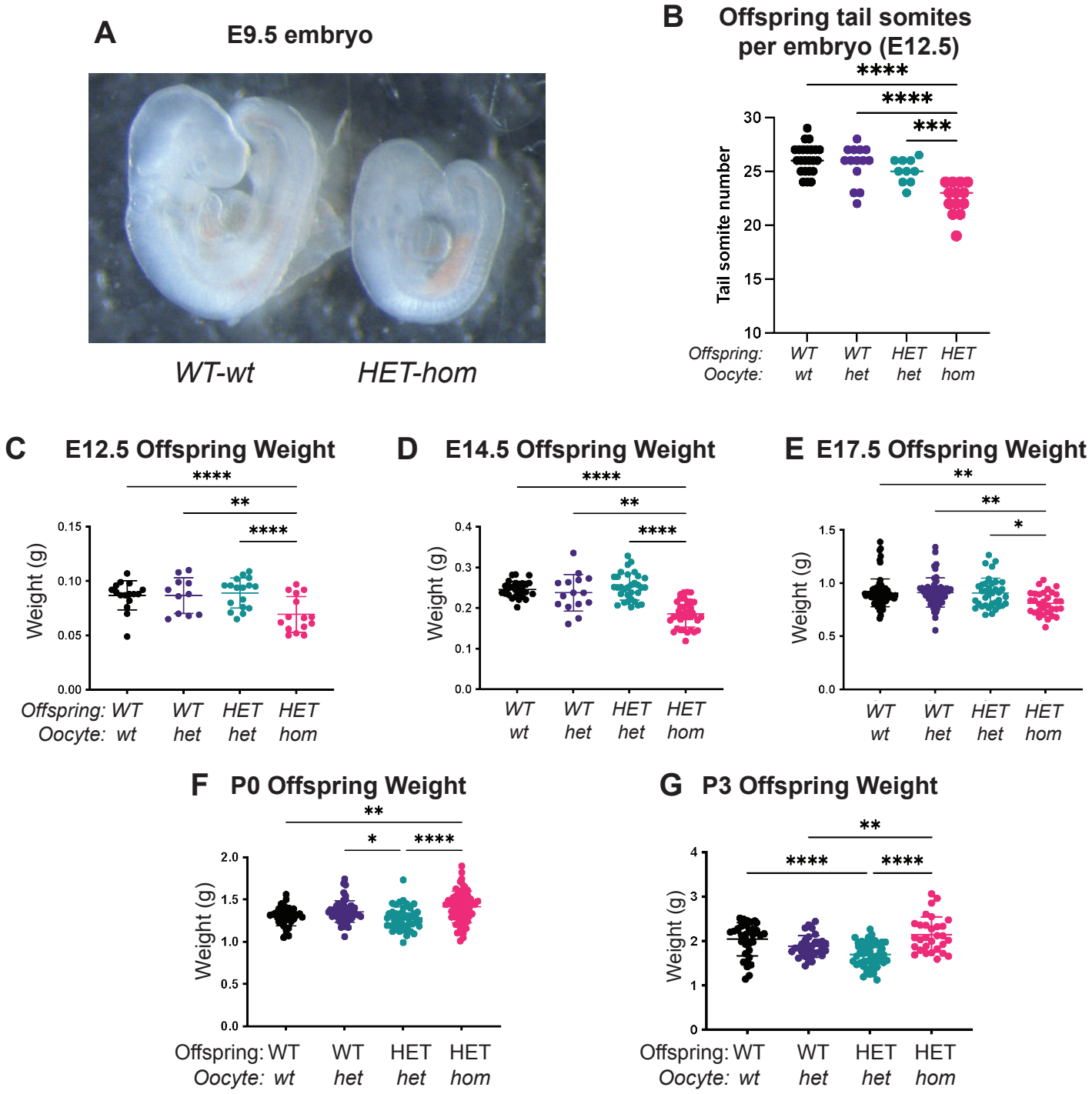
A
E9.5 embryo
WT-wt
HET-hom
B
Offspring tail somites per embryo (E12.5)
Tail somite number
Offspring: WT WT HET HET
Oocyte: wt het het hom
C
E12.5 Offspring Weight
Weight (g)
D
E14.5 Offspring Weight
E
E17.5 Offspring Weight
F
P0 Offspring Weight
G
P3 Offspring Weight

Figure 2

858 **Figure 2. Loss of EED-dependent oocyte programming resulted in fetal loss and offspring**
859 **developmental delay. (a)** Representative wholemount images of E9.5 embryos. **(b)** Number
860 of tail somites in E12.5 *WT-wt, WT-het*, *HET-het* and *HET-hom* embryos. ****P<0.0001,
861 ***P<0.0005, N=10-23/genotype. **(c-g)** Offspring body weight at E12.5, E14.5, E17.5 and P0.
862 ****P<0.0001, ***P<0.0005, **P<0.005, N=15-75/genotype. **(b-g)** statistically analysed using
863 one-way ANOVA plus Tukey's multiple comparisons.
864

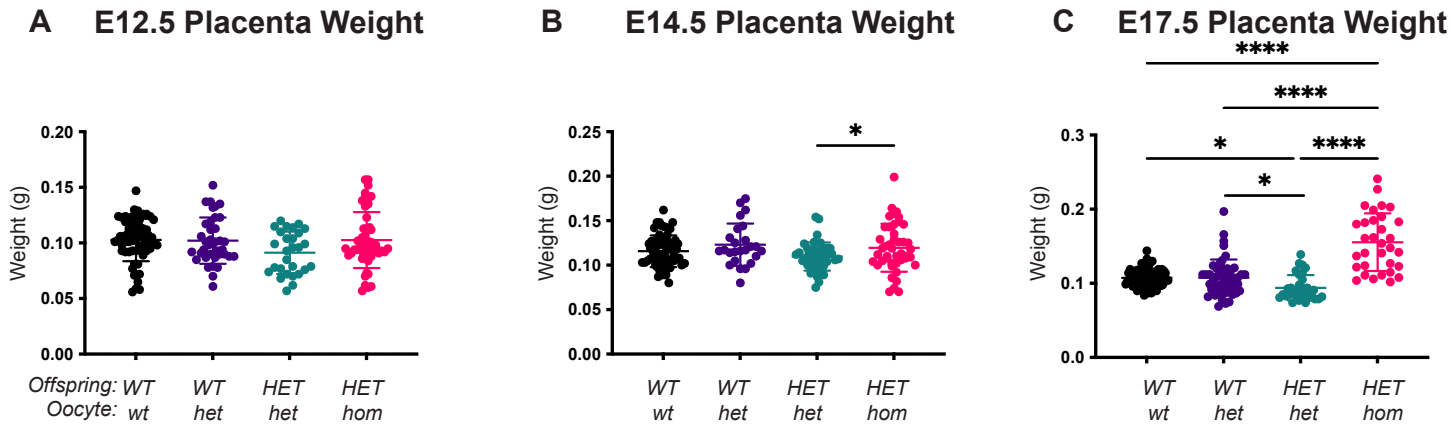

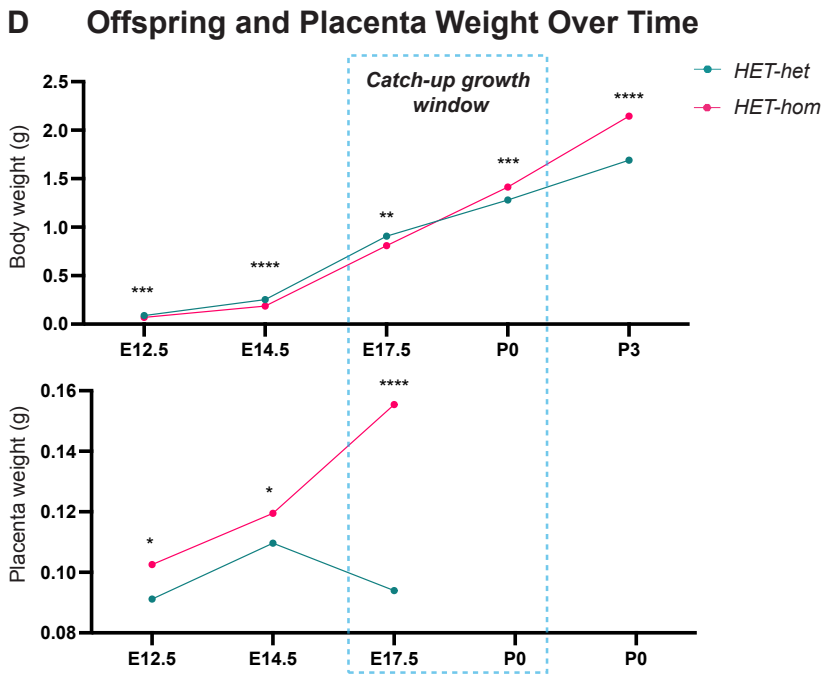

E Placental growth rate (weight change/time)

	HET-het	*HET-hom*
E12.5-E14.5	0.00921	0.00845
E14.5-E17.5	-0.00522	0.0119667

F Offspring growth rate (weight change/time)

	HET-het	*HET-hom*
E12.5-E14.5	0.08191	0.058235
E14.5-E17.5	0.2183333	0.2079
E17.5-E19.5/P0	0.18615	0.27475

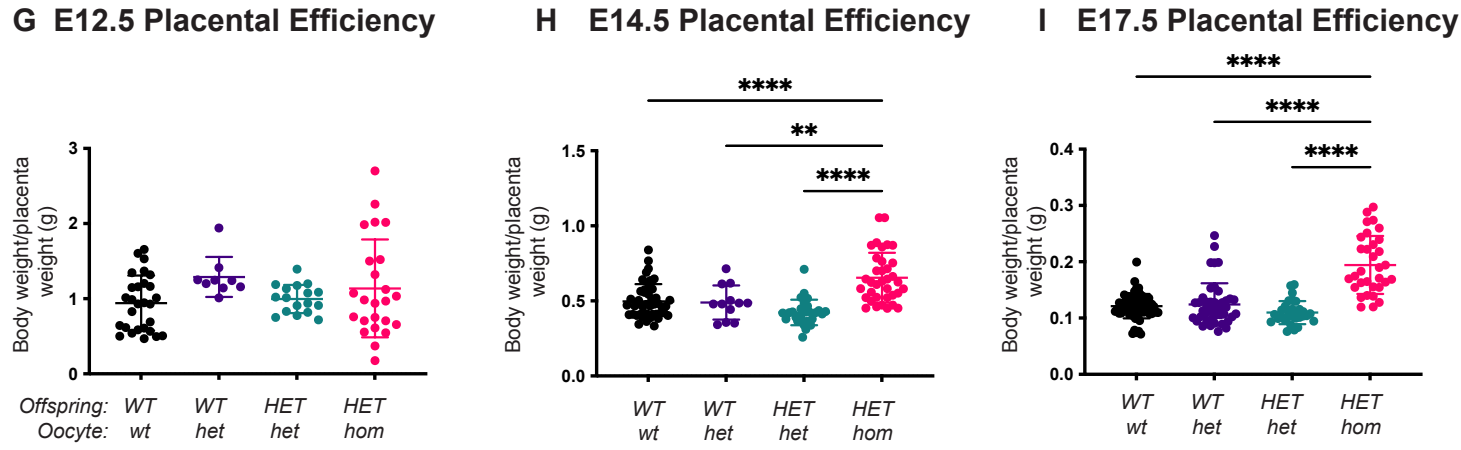

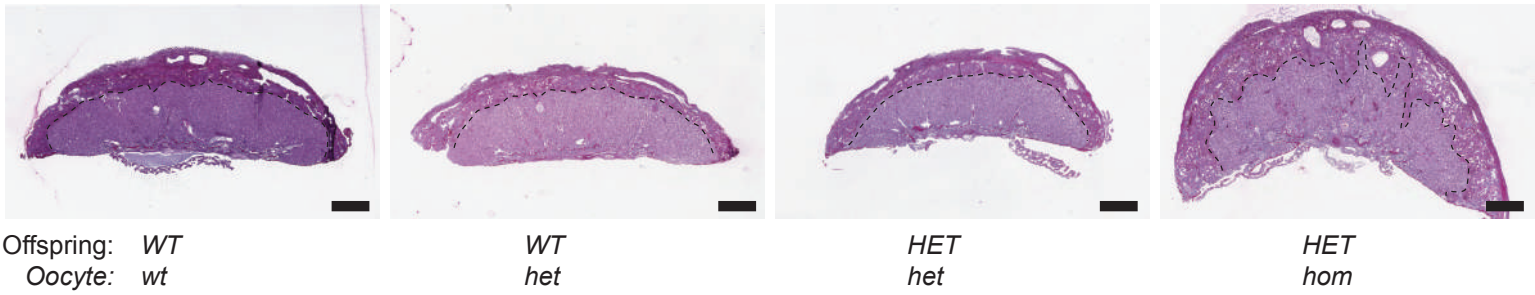

Figure 3

865 **Figure 3. Placental differences were observed in heterozygous offspring from oocytes that**
866 **lacked *Eed.* (a-c)** Placental weight at E12.5, E14.5 and E17.5 ****P<0.0001, *P<0.05, N=32-
867 68/genotype. **(d)** Isogenic heterozygous offspring and placenta average weight over time.
868 *P<0.05, **P<0.005, ***P<0.0005, ****P<0.0001 unpaired t-test, N=28-56/genotype. **(e-f)**
869 Tables depicting *HET-het* and *HET-hom* offspring and placenta growth rates across 2-3 time
870 points throughout gestation. **(g-i)** Ratio of placental weight to offspring body weight at E12.5,
871 E14.5 and E17.5. ****P<0.0001, **P<0.005, N=9-66/genotype. **(j)** Placental cross-sections at
872 E17.5 stained with PAS. Scale bars= 800µm. **(a-c, g-i)** statistically analysed using one-way
873 ANOVA plus Tukey's multiple comparisons.
874

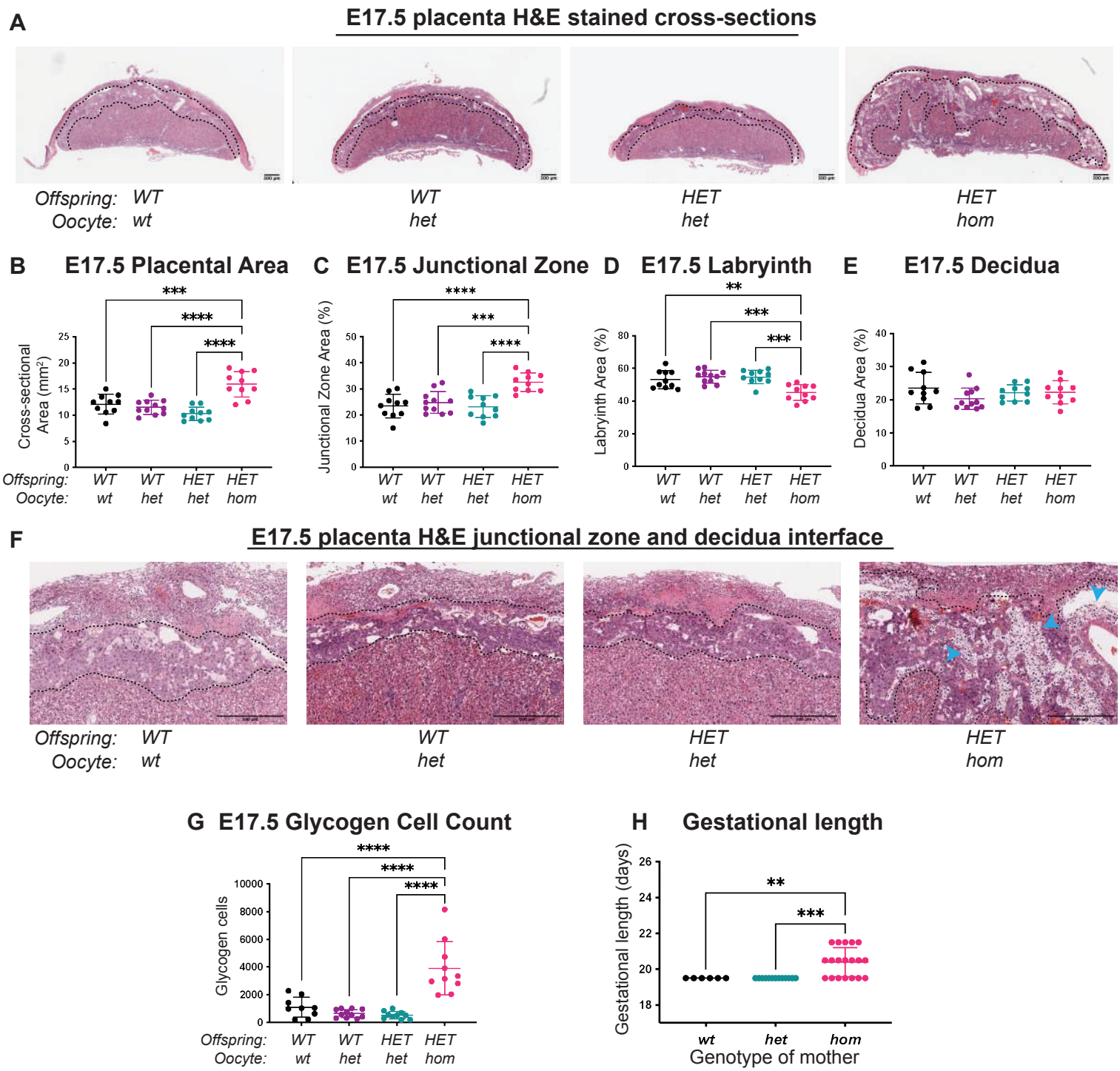
A
E17.5 placenta H&E stained cross-sections
Offspring: WT WT HET HET
Oocyte: wt het het hom
B E17.5 Placental Area
Cross-sectional Area (mm²)
C E17.5 Junctional Zone
Junctional Zone Area (%)
D E17.5 Labryinth
Labryinth Area (%)
E E17.5 Decidua
Decidua Area (%)
F
E17.5 placenta H&E junctional zone and decidua interface
G E17.5 Glycogen Cell Count
Glycogen cells
H Gestational length
Gestational length (days)
Genotype of mother

Figure 4

875 **Figure 4. Complete deletion of *Eed* in the oocyte resulted in offspring altered placental**
876 **morphology and gestational length. (a)** Placental cross-sections at E17.5 stained with H&E,
877 black dotted line indicates the borders between labyrinth, junctional zone and decidual
878 layers. Images are representative of an individual placenta typical of each genotype, with 10
879 biological replicates analysed/genotype. Scale bars= 500µm. **(b)** Placental cross-sectional area
880 at E17.5. ***P<0.0005, ****P<0.0001, N=10/genotype. **(c-e)** Area of E17.5 junctional zone,
881 labyrinth and decidua. **P<0.01, ***P<0.001, ****P<0.0001, N=10/genotype. **(f)**
882 Representative images of E17.5 junctional zone stained with H&E. Blue arrowheads, glycogen
883 cells. Scale bars= 500µm. **(g)** Quantification of total number of glycogen cells in E17.5 placenta
884 cross section. ****P<0.0001, N=10/genotype. **(h)** Gestational length for females producing
885 litters from *Eed-wt, Eed-het* and *Eed-hom* oocytes. **P<0.01, ***P<0.001, N=6 litters from
886 *Eed-wt* oocytes, N=13 litters from *Eed-het* oocytes and N=19 litters from *Eed-hom* oocytes.
887 **(b-e, g-h)** statistically analysed using one-way ANOVA plus Tukey's multiple comparisons.
888

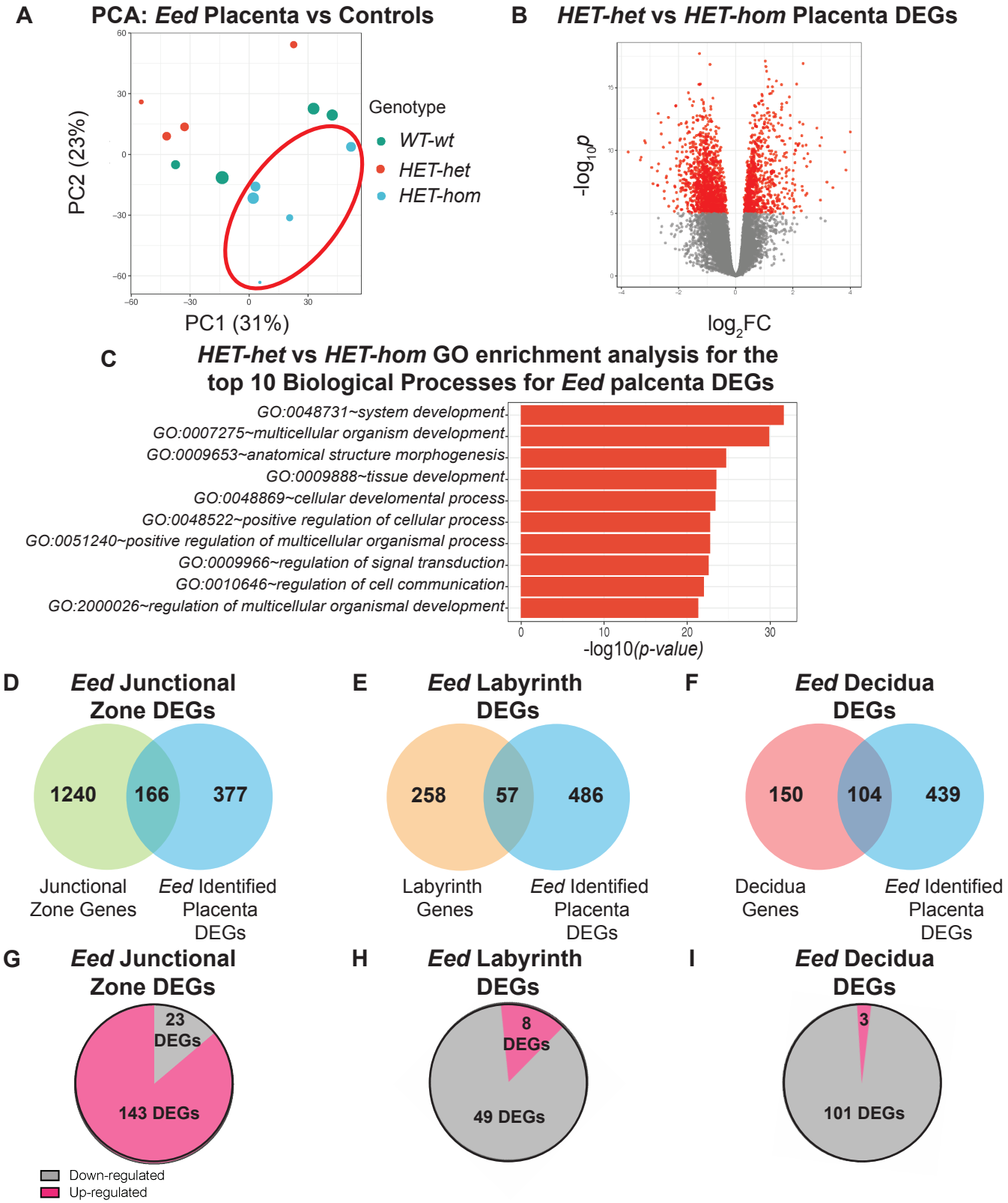
A
PCA: Eed Placenta vs Controls
PC2 (23%)
PC1 (31%)
Genotype
WT-wt
HET-het
HET-hom
B
HET-het vs HET-hom Placenta DEGs
-log10p
log2FC
C
HET-het vs HET-hom GO enrichment analysis for the top 10 Biological Processes for Eed palcenta DEGs
GO:0048731~system development
GO:0007275~multicellular organism development
GO:0009653~anatomical structure morphogenesis
GO:0009888~tissue development
GO:0048869~cellular developmental process
GO:0048522~positive regulation of cellular process
GO:0051240~positive regulation of multicellular organismal process
GO:0009966~regulation of signal transduction
GO:0010646~regulation of cell communication
GO:2000026~regulation of multicellular organismal development
-log10(p-value)
D
Eed Junctional Zone DEGs
1240
166
377
Junctional Zone Genes
Eed Identified Placenta DEGs
E
Eed Labyrinth DEGs
258
57
486
Labyrinth Genes
Eed Identified Placenta DEGs
F
Eed Decidua DEGs
150
104
439
Decidua Genes
Eed Identified Placenta DEGs
G
Eed Junctional Zone DEGs
23 DEGs
143 DEGs
H
Eed Labyrinth DEGs
8 DEGs
49 DEGs
I
Eed Decidua DEGs
3
101 DEGs
Down-regulated
Up-regulated

Figure 5

889 **Figure 5. Loss of EED-dependent oocyte programming altered transcription in female *HET-***
890 ***hom* placenta. (a)** Principal Component Analysis (PCA) for female *HET-hom*, *HET-het* and *WT-*
891 *wt* placenta. N=4-5/genotype. **(b)** Differential gene expression analysis of isogenic *HET-het* vs
892 *HET-hom* placenta represented by a volcano plot showing logFC against statistical
893 significance. Genes with FDR-adjusted FDR<0.05 are coloured in red. Deletion of *Eed* in the
894 oocyte resulted in 2083 DEGs in *HET-hom* placenta (*Eed* placental DEGs). **(c)** GO enrichment
895 analysis of *HET-het* vs *HET-hom* DEGs representing the top 10 significantly different biological
896 processes impacted (**d-f)** Venn diagrams showing comparisons of: **(d)** identified junctional
897 zone genes vs *Eed* identified placenta DEGs, **(e)** identified labyrinth genes vs *Eed* identified
898 placenta DEGs, **(f)** identified decidua genes vs *Eed* identified placenta DEGs. **(g-i)** pie graph
899 depicting the distribution of up-regulated (pink) and down-regulated (grey) *Eed* DEGs
900 identified to be expressed in **(g)** junctional zone, **(h)** labyrinth and **(i)** decidual layer of mouse
901 placenta.
902

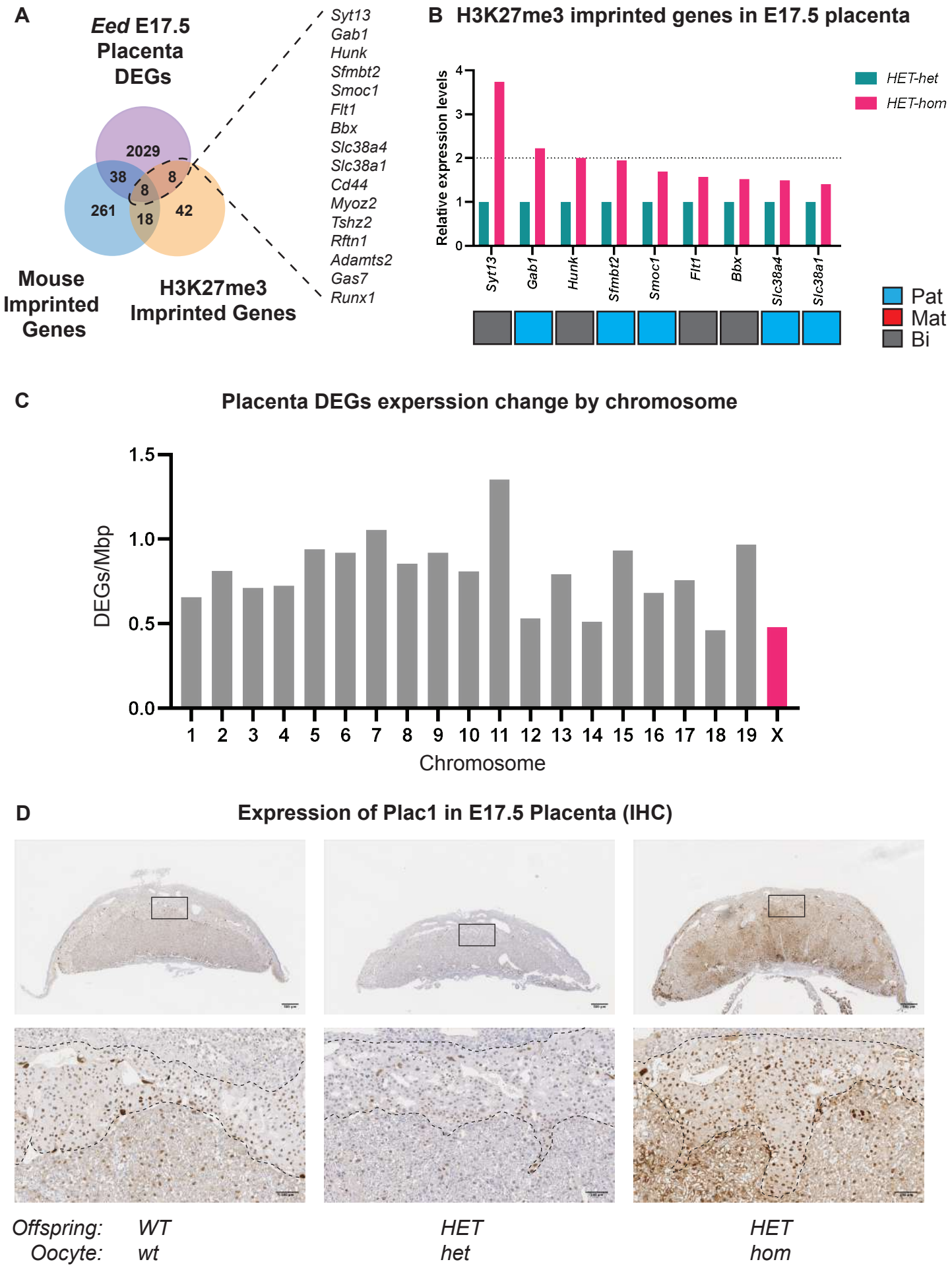
A
Eed E17.5 Placenta DEGs
2029
38
8
8
261
18
42
Mouse Imprinted Genes
H3K27me3 Imprinted Genes
Syt13
Gab1
Hunk
Sfmbt2
Smoc1
Flt1
Bbx
Slc38a4
Slc38a1
Cd44
Myoz2
Tshz2
Rftn1
Adamts2
Gas7
Runx1
B H3K27me3 imprinted genes in E17.5 placenta
Relative expression levels
HET-het
HET-hom
Syt13
Gab1
Hunk
Sfmbt2
Smoc1
Flt1
Bbx
Slc38a4
Slc38a1
Pat
Mat
Bi
C
Placenta DEGs experssion change by chromosome
DEGs/Mbp
Chromosome
D
Expression of Plac1 in E17.5 Placenta (IHC)
Offspring: WT HET HET
Oocyte: wt het hom

Figure 6

903 **Figure 6. Loss of EED in the oocyte results in the de-repression of imprinted and X-linked**
904 **genes. (a)** Venn diagram showing comparisons of *Eed* placenta DEGs vs known mouse
905 imprinted genes (37, 38)(bottom left) and H3K27me3 imprinted genes (22) (bottom right). **(b)**
906 Relative expression levels of H3K7me3 imprinted genes that were upregulated in female
907 E17.5 *HET-hom* placenta compared to female *HET-het* control (FDR<0.05). **(c)** *Eed* placental
908 DEG distribution across the genome, represented as DEGs/Mbp for all autosomes and the X-
909 chromosome. **(d)** Representative images of PLAC1 expression in E17.5 female placenta,
910 N=4/genotype. Scale bars= 500µm (top), scale bars= 100µm (bottom).
911

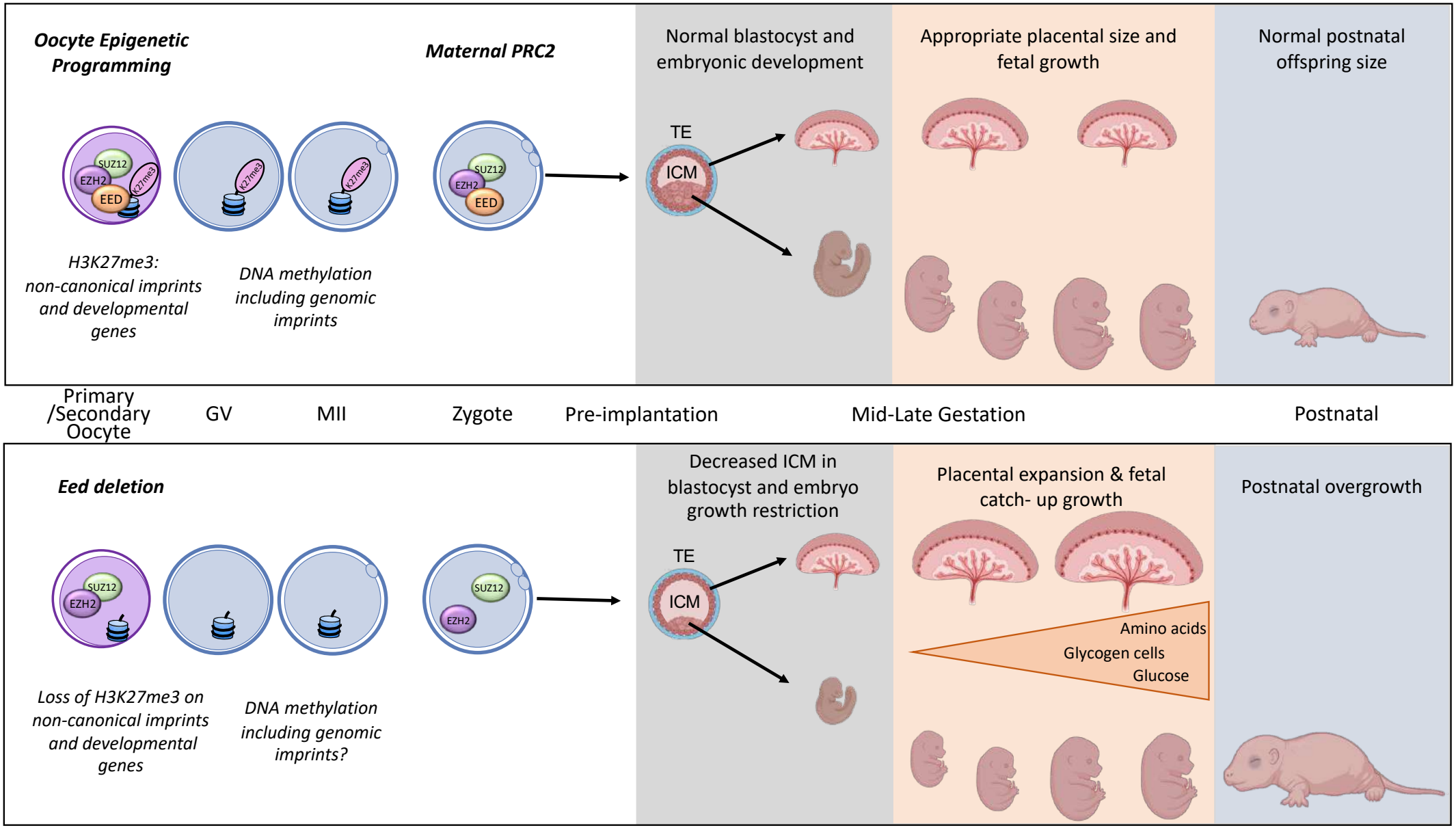
Oocyte Epigenetic Programming
Maternal PRC2
Normal blastocyst and embryonic development
Appropriate placental size and fetal growth
Normal postnatal offspring size
SUZ12
EZH2
EED
K27me3
TE
ICM
H3K27me3: non-canonical imprints and developmental genes
DNA methylation including genomic imprints
Primary /Secondary Oocyte
GV
MII
Zygote
Pre-implantation
Mid-Late Gestation
Postnatal
Eed deletion
Decreased ICM in blastocyst and embryo growth restriction
Placental expansion & fetal catch- up growth
Postnatal overgrowth
Amino acids
Glycogen cells
Glucose
Loss of H3K27me3 on non-canonical imprints and developmental genes
DNA methylation including genomic imprints?

Figure 7

912 **Figure 7. Summary of the placental and offspring growth response due to EED loss in the**
913 **oocyte.** During oocyte growth all three subunits of PRC2 are present at the primary to
914 secondary stages, which is important for the silencing of developmental genes and
915 H3K27me3-dependent imprinting (Jarred et al., 2022, submitted). Deletion of *Eed* in oocyte
916 results in loss of maternal H3K27me3 and PRC2, early growth restriction, followed by
917 placental hyperplasia and late gestation fetal catch-up growth, outcomes consistent with loss
918 of H3K27me3-dependent imprinting observed in SCNT offspring (25-27). Placentas generated
919 from oocytes lacking EED have expanded glycogen enriched cells in the junctional zone and
920 significant gene dysregulation in the placenta. Placental hyperplasia immediately precedes
921 rapid fetal catch-up growth, explaining why these offspring are overgrown immediately after
922 birth (7). Figure created with BioRender.com.
923
924

925

926 ***Supplementary Data and Information***

927

928 ***Loss of EED in the oocyte causes initial fetal growth restriction followed by placental***

929 ***hyperplasia and offspring overgrowth.***

930

931 **Short title:** *Epigenetic regulation of fetal growth restriction, placental expansion and*
932 *offspring overgrowth*
933
934
935 **Authors:** Ruby Oberin[1#], Sigrid Petautschnig[1#], Tesha Tsai[1^], Zhipeng Qu[2], Ellen G. Jarred[1],
936 Heidi Bildsoe[1], Thi T. Truong[3], Dilini Fernando[1], Maarten van den Buuse[4], David K. Gardner[3],
937 Natalie A. Sims[5], David L. Adelson[2] and Patrick S. Western[1]*
938
939
940
941
942 **Supplementary Tables** can be found in associated Excel File: Oberin and Petautschnig *etal.*
943 Supplementary Tables
944
945
946 **Supplementary Figures** are found below

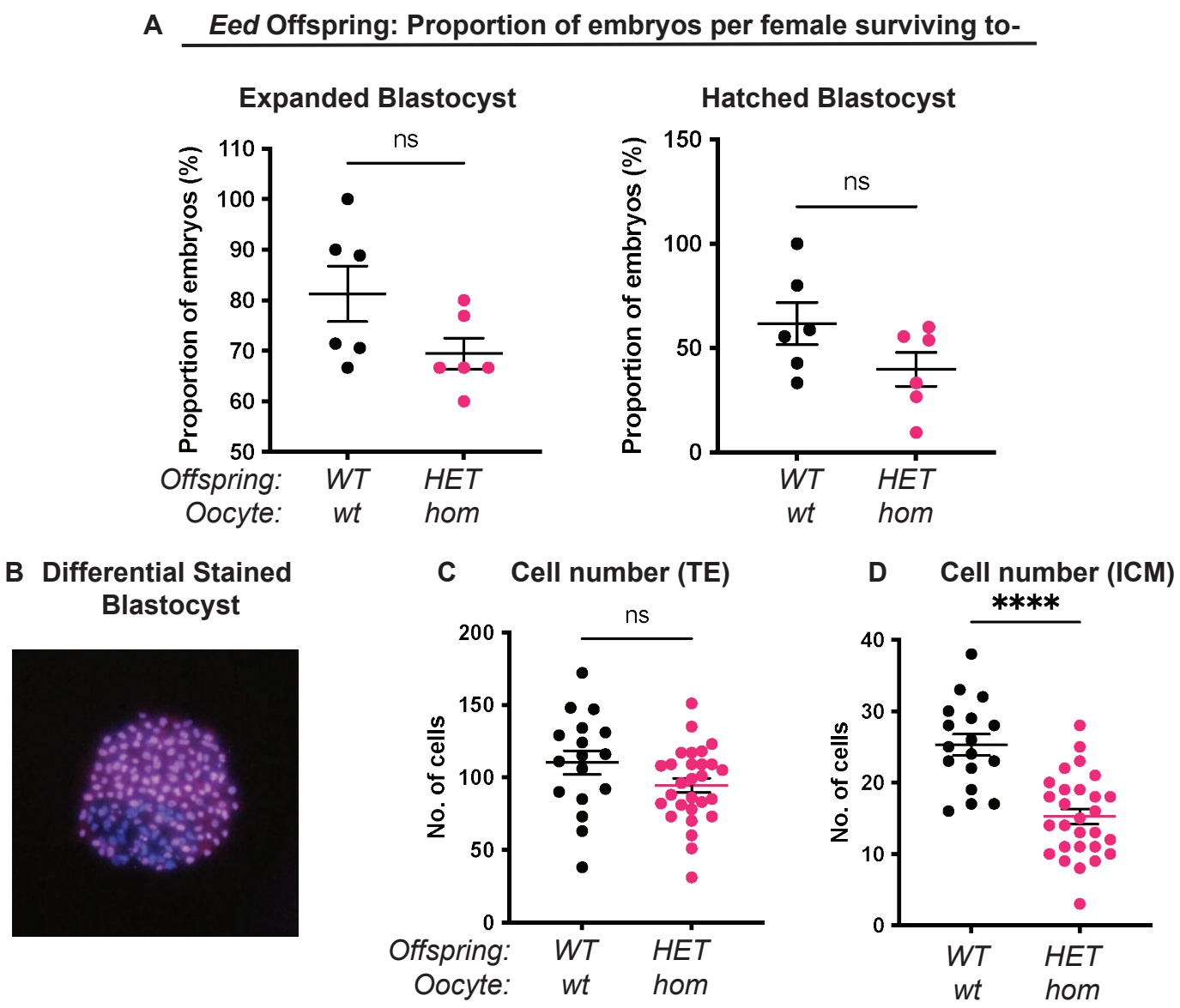

Supp. Figure 1

947 **Supplementary Figure Legends**

948 **Supplementary Figure 1. Maternal *Eed* deletion impacted pre-implantation development.**
949 **(a)** Proportion of embryos from *Eed-wt* or *Eed-hom* oocytes surviving to expanded blastocyst
950 (left) and hatched blastocyst (right). Data represent the proportion of surviving embryos from
951 each female, N = 6 females. **(b)** Example of a differentially stained blastocyst that has been
952 treated with propidium iodide followed by bisbenzimide to identify purple cells representing
953 inner cell mass (ICM) and pink cells representing trophectoderm (TE). **(c)** Number of TE cells
954 per embryo. ns = no significant difference, $P > 0.05$, N = 17 embryos from *Eed-wt* oocytes, 28
955 embryos from *Eed-hom* oocytes. **(d)** Number of ICM cells per embryo. ****$P < 0.0001$, N = 17
956 embryos from *Eed-wt* oocytes, 28 embryos from *Eed-hom* oocytes. For **(a, c-d)** a two-tailed
957 student's t test was used, and error bars represent mean ± SD.

958

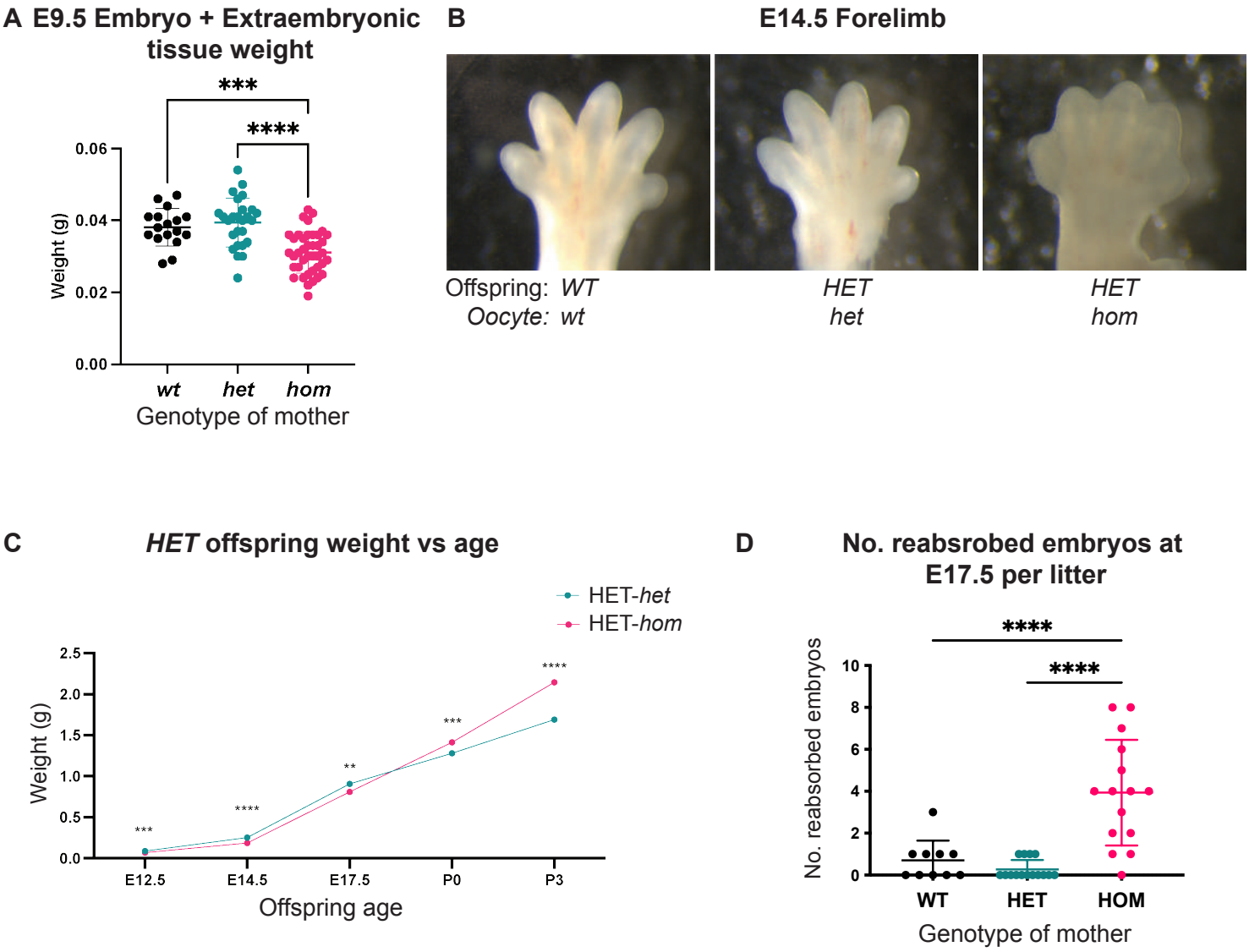

Supp. Figure 2

959 **Supplementary Figure 2. Loss of EED-dependent oocyte programming resulted in altered**
960 **fetal and neonatal development. (a)** Embryo and extraembryonic tissue weight at E9.5.
961 ****P<0.0001, ***P<0.0005, N=17-40/genotype. **(b)** Representative wholemount images of
962 E14.5 forelimbs revealing reduced inter-digital tissue regression in *HET-hom* offspring. **(c)**
963 Isogenic heterozygous offspring average weight over time. ***P<0.0005, ****P<0.0001
964 unpaired t-test, N=28-56/genotype. **(d)** Number of reabsorbed embryos per litter at E17.5.
965 ****P<0.0001 N=10-15 litters/genotype. **(a, c, e,)** statistically analysed using one-way ANOVA
966 plus Tukey's multiple comparisons.
967

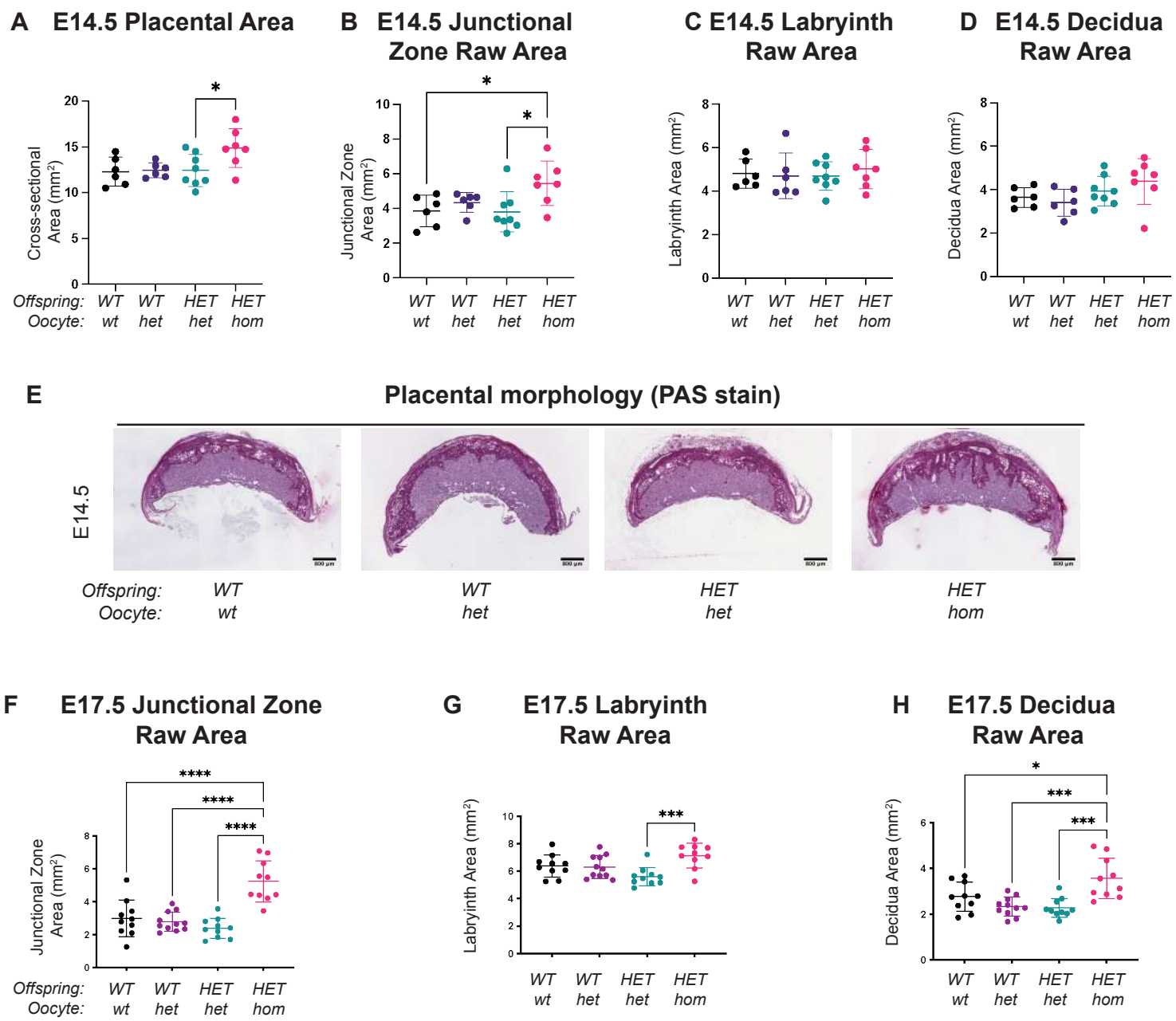

Supp. Figure 3

968 **Supplementary Figure 3. Complete deletion of *Eed* in the oocyte resulted in altered**
969 **placental size. (a)** E14.5 placenta cross-sectional area. *P<0.05, N=10/genotype. **(b-d)** Raw
970 area of E14.5 junctional zone, labyrinth and decidua. *P<0.05, N=10/genotype. **(e)** Placental
971 cross-sections at E14.5 stained with PAS. Scale bars= 800µm. **(f-h)** Raw area of E17.5
972 junctional zone, labyrinth and decidua. ****P<0.0001, ***P<0.0005, *P<0.05,
973 N=10/genotype. Statistically analysed using one-way ANOVA plus Tukey's multiple
974 comparisons.
975

Supp. Figure 4

976 **Supplementary Figure 4. Loss of EED-dependent oocyte programming altered transcription**
977 **in male *HET-hom* placenta. (a)** Principal Component Analysis (PCA) for *HET-hom*, *HET-het*
978 and *WT-wt* placenta. N=3-4/genotype. **(b)** Differential gene expression analysis of isogenic
979 *HET-het* vs *HET-hom* placenta represented by a MD plot showing $\log_2$FC against statistical
980 significance. Gene with FDR-adjusted FDR<0.05 is coloured in red. Deletion of *Eed* in the
981 oocyte resulted in one DEG in male *HET-hom* placenta.
982

A X-linked and imprinted genes in E17.5 placenta

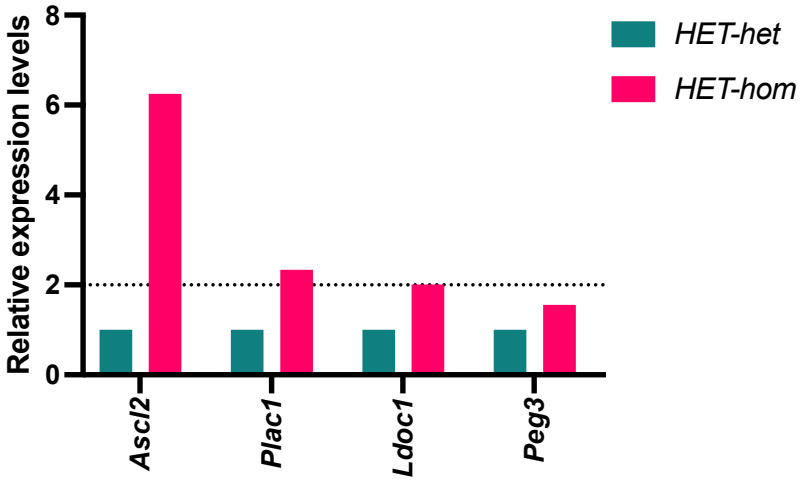

Supp. Figure 5

983 **Supplementary Figure 5. Loss of EED in the oocyte results in the de-repression of X-linked**
984 **and imprinted genes that are important for placental development. (a)** Relative expression
985 levels of X-linked and imprinted genes in female E17.5 *HET-hom* placenta compared to female
986 *HET-het* control (FDR<0.05).
987

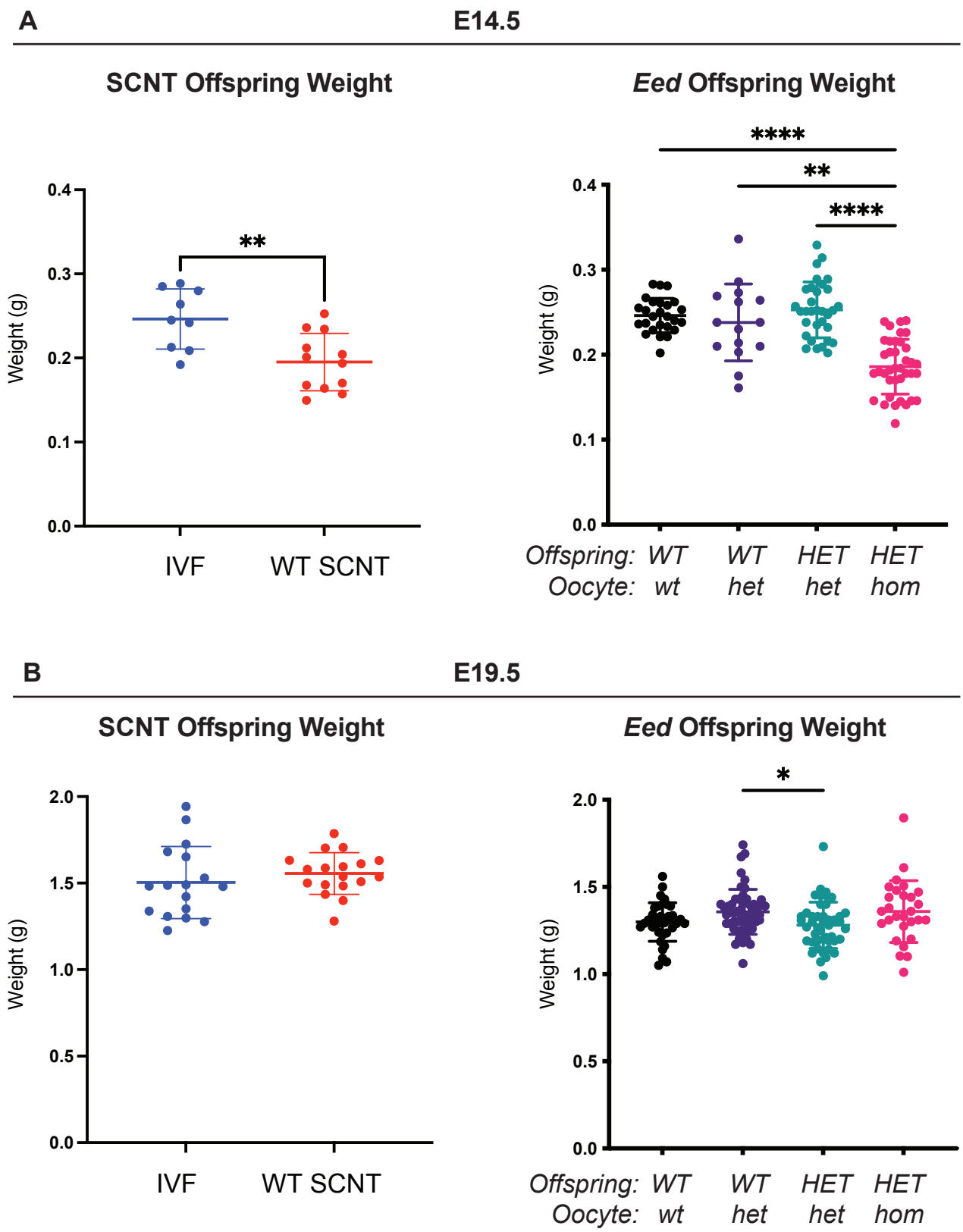

Supp. Figure 6

988 **Supplementary Figure 6. *HET-hom* offspring demonstrate similar growth profiles to SCNT**
989 **mice.** Comparison of body weights of SCNT mice from Xie, Zhang (27) and offspring from the
990 *Eed-ZP3*-Cre mouse model at **(a)** E14.5 and **(b)** E19.5. ****P<0.0001, **P<0.005 and *P<0.05.
991 Statistically analysed using one-way ANOVA plus Tukey's multiple comparisons.
992